

Z (1936



This is to certify that the

thesis entitled

Ch. Examination of the Relationship between
Thage Processed Electron Back Scattered
Patterns and Plastic Strain in Bulk
aluminum materials

presented by

Ojars Balcers

has been accepted towards fulfillment
of the requirements for

master's degree in Materials decided to the second second

Major professor

# LIBRARY Michigan State University

PLACE IN RETURN BOX to remove this checkout from your record.

TO AVOID FINES return on or before date due.

DATE DUE	DATE DUE	DATE DUE

MSU is An Affirmative Action/Equal Opportunity Institution

# AN EXAMINATION OF THE RELATIONSHIP BETWEEN IMAGE PROCESSED ELECTRON BACK SCATTERED PATTERNS AND PLASTIC STRAIN IN BULK ALUMINUM MATERIALS

Ву

Ojars Balcers

#### **A THESIS**

Submitted to
Michigan State University
in partial fulfillment of the requirements
for the degree of

MASTER OF SCIENCE

Department of Materials Science and Mechanics

#### **ABSTRACT**

# AN EXAMINATION OF THE RELATIONSHIP BETWEEN IMAGE PROCESSED ELECTRON BACK SCATTERED PATTERNS AND PLASTIC STRAIN IN BULK ALUMINUM MATERIALS

By

#### Ojars Balcers

This study measured microscale plastic strain deformation of bulk aluminum materials. The initial objective of this research program was to improve the quality of electron backscattered patterns (EBSPs) obtained on the Hitachi S-2500 SEM. It is shown that SEM generated EBSPs can be used to characterize the plastic strain of materials at the micron-scale. The pattern's diffuseness increases with increased departure from perfect lattice crystallinity.

Two experimental configurations are described. Both configurations include a signal processing stage and are used to characterize EBSP quality. One configuration compares patterns qualitatively, but in real-time, using a video camera; the other configuration does not work in real-time, but has the advantage of acquiring high quality EBSPs for semi-quantitative measurements and uses a remotely controlled photo camera. The steps for acquiring good quality samples are reviewed. The results of two quantification methods are analyzed.

# **DEDICATION**

To my Mom and Dad
for love and support, and for believing and helping to make this possible,
to EDĪTE
for the very motivating looking up,
and to my grandparents
for their love, care, and strength.

#### **ACKNOWLEDGMENTS**

In the first place, I would like to acknowledge my entire family for their love, support, belief and encouragement. Without them (Mom and Dad, Kristine and Edite, John and Cathy) this thesis hardly would be possible. I would also like to acknowledge Prof. Martin A. Crimp, my advisor, for finding funding for my project, keeping true interest in it, and his advisement on electron microscopy, sample preparation, and photography, but especially for being most understanding during the deep and prolonged crisis in my personal life during the final stage of the project. I also must thank Alan Gibson with whom we worked together on various stages on developing and materializing this research program and finally achieved valuable results, and who simply was a great person. Dave, Julian, Ben, Keith, Todd, Cris, John, Marilyn, Girts, Donna, Kayoko, Iveta and Arvydas were my "brothers-in-arms", and that important safety and prompt advice net, when I needed it.

I gratefully acknowledge contribution of Dr. Brian Cantor, my research supervisor in Oxford, who's guidance helped me to evolve as a scientist and made me understand that science is about constant learning, hard work, and, most important, people. Also, I gratefully acknowledge Dr. Angus J. Wilkinson's advice on image manipulations.

I must also acknowledge my gratitude to my former teachers in Riga, Latvia - Mr. Dainis Krikis, Prof. Aivars Simanovskis, Dr. Pauls Stradins, and Prof. Kurts Svarcs.

# **TABLE OF CONTENTS**

	Page
LIST OF FIGURES	vii
KEY TO SYMBOLS AND ABBREVIATIONS	хi
INTRODUCTION	. 1
LITERATURE REVIEW	3
1.1. Use of the EBSP method	. 3
1.2. Physical principles of pattern formation	. 6 . 7
1.3. Digital image enhancement	. 11
1.3.1. LINK digital processing 1.3.2. Differential signal amplification (contrast expansion) 1.3.3. Frame averaging 1.3.4. Histogram modification 1.3.5. Spatial-domain techniques (averaging, median filtering, background subtraction) 1.3.6. Frequency-domain methods 1.3.7. Image restoration 1.3.7.1. Interactive restoration 1.3.7.2. Restoration in the spatial domain	. 14 . 16 . 17 . 21 . 24
1.4. EBSP quantification mathematical aspects	27
EXPERIMENTAL PROCEDURE	. 33
2.1. Sample deformation	33

2.2. Surface prep	paration	35
2.3. EBSP collec	tion	39
RESULTS AND	DISCUSSION	41
_	aquisition system development with SEMPER 6.4 software BSP capture using a videocamera and the LINK system	41 46
3.3. Correlation l	between the surface quality and the EBSPs	51
3.4. High quality	patterns acquisition using a fine grain photofilm and a scanner	56
3.5.1. Spectra 3.5.2. Power 3.5.3. Evalua	iness quantification	61 63 67 72
CONCLUSIONS		75
RECOMMENDA	ATIONS	76
APPENDIX A	Correct semper.run file to account for European TV signal	77
APPENDIX B	Semper image processing software summary	78
APPENDIX C	Live EBSP capture and processing Semper commands used	83
APPENDIX D	1-D SFPA quantification Semper commands used	84
APPENDIX E	2-D PSFM quantification Semper commands used	85
LIST OF REFER	ENCES	86

# **LIST OF FIGURES**

<u>Figure</u>		<u>Page</u>
1.	EBSP formation (a) illustration of the set up to produce images, (b) an EBSP pattern with the first and higher order lines present.	4
2.	Electron emission profiles (after [11], quoting Laponsky, Whetten, Alam) (a) from amorphous materials, (b) from crystalline materials, (c) the geometry for the production of EBSPs.	7
3.	Monte-Carlo simulation predicted effects (after [11], quoting Newbury, Myklebust, Heinrich) (a) dependence of the backscattered electron coefficient (BSE) on specimer (b) dependence of BSE coefficient on atomic number of the target; $E = 20 \text{ M}$	
4.	Multimode scanning electron microscopy [11] (a) point resolution along a line scan. Two points are resolved when $B_{max} - \Delta B \le 0.75 \ B_{max}$ or $\Delta B \ge 0.25 \ B_{max}$ , (b) a signal line scan trace without back-off and with back-off and increase amplifier gain, (c) if the spatial detection limit is $d$ and the point brightness peak is of squawaveform, the contrast minimum between adjacent bright points rises sudd	ire
5.	Illustration of a scan line trace across an image. "A" and "B" are two arbitrarily chosen points.	15
6.	Illustration of the histogram-equalization approach [28] (a) original image, (b) original histogram, (c) equalized histogram, (d) enhanced image.	18
7.	Illustration of the histogram-specification method [28] (a) original image, (b) histogram - equalized image, (c) image enhanced by histogram specification, (d) histograms.	19

<u>Figure</u>		<u>Page</u>
8.	Image smoothing by averaging and median filtering [28] (a) original image, (b) image corrupted by impulse noise, (c, d) result of 5 x 5 neighborhood averaging, and 5 x 5 median filtering of the corrupted image.	20
9.	Lowpass filters [28] (a) 256 x 256 pixel image, (b) its 2-D Fourier spectrum. The superimposed circles, which have radii 5, 11, 22, 36, 53, and 98 enclose 90, 95, 98, 99, 99.5, and 99.9% of image (c-h) results of applying ideal lowpass filters to (a). Radii 5-98 correspondence.	power,
10.	Example of highpass filtering [28] (a) original image, (b) result of high-frequency emphasis, i.e., highpass filtering, (c) high-frequency emphasis and histogram equalization.	23
11.	Example of interactive restoration by sinusoidal interference removal [28] showing (a) a model of the degradation process, (b) a corrupted image, (b) a Fourier spectrum showing impulses due to sinusoidal pattern, and (c) an image restored by using a band-reject filter with radius of one.	25
12.	Restoration in the spatial domain [28] demonstrating (a) an infrared image showing interference, (b) an image restored using a notch filter in the frequency domain, (c) a Fourier spectrum of the image in (a), and (d) a notch filter superimposed on the spectrum.	26
13.	Fourier transform properties (after [35, 36]) (a) Fourier transform pairs show the emphasis of the Fourier transform central peak as the original changes from the rectangular to the more "diffuse" bell-shape form, (b) the first moment, $\sum x f(x)$ , characterize function's $f(x)$ distribution along The impulse pair's first moment is $1/4 = (-1/2) \times (-1/2) + 1/2 \times 1/2$ .	28 g a line

<u>Figure</u>	Pag	<u>ge</u>
14.	Digital filter characteristics (after [34], quoting Bruel and Kjaer Instruments) (a) graphic displays of four common window functions (rectangular, Haning, Kaiser-Bessel, and flat-top) in the time domain. The area under each window function is unity, (b-e) filter shapes for weighting with (b) rectangular, (c) Hanning, (d) Kaiser-Bessel, (e) flat-top window functions.	31
15.	Electrolytic polishing technique  (a) a simple electropolishing cell,  (b) general form of the relation between cell voltage and anode current density Regions relate to the following anodic processes: A-B etching; B-C instability C-D polishing; D-E slow gas evolution with pitting; E-F polishing with rapid gas evolution. P indicates optimum polishing conditions.	•
16.	Semper "live" command captured EBSPs of electropolished Al (a) captured single frame, (b) image enhanced by recursive filtering over 30 sec, (c) same as in (b), after background ramp removal and histogram equalization	42
17.	Real time EBSPs capturing configuration.	45
18.	LINK system simulated aluminum EBSP map.  Accelerating voltage = 20 kV, angular width = 90 deg, central zone = <112>.  A rectangle is drawn around the area that is used for quantification.	48
19.	Digitizing and enhancing algorithm used in LINK controlled TV camera live capture of EBSP images. Semper commands are presented in the Appendix C.	50
20.	Electron discharge machine spark's energy influence on the Al samples EBSP's quality  (a) optical micrograph of the cut with the lowest available spark energy (setting (b) optical micrograph of the cut with higher spark energy (setting 3), (c) corresponding EBSP pattern obtained from surface (b) with the LINK syst (only background noise is present in EBSPs corresponding to (a)).	
21.	High quality EBSP's capturing configuration (a) photocamera and sample geometry in the SEM chamber, (b) overall system layout.	57
22.	Signal processing algorithm used in slide digitizing.	59

Figure	<u>Page</u>

23.	Representative Al EBSPs at different steps of digitizing (a) an EBSP as scanned, (b) same as in (a) after rotation, cropping and automatic level adjustment, (c) same as in (b) after extracting a 256 x 256 p square and resetting outliers, (d) same as in (c) after removing the ramp and image stretching. Image mean is set to zero.	
24.	Indexing of aluminum (fcc) bands around the <112> zone. The white line depicts the line along which (the $(\overline{3}11)$ band) the patterns were extracted in the 1-D SFPA case.	62
25.	Electron back scattered pattern quantification algorithm.	64
26.	EBSP patterns from 99.999% purity Al deformed in compression to (a) 0%, (b) 5%, (c) 14%, and (d) 18%. All patterns are extracted around the <112> zone. The patterns tend to "diffuse out" with the increase of applied strain to the polycrystalline aluminum.	65
27.	Average intensity profiles of $(\overline{3}11)$ bands present in EBSPs obtained from (a) annealed and (c) 18% strained polycrystalline aluminum. The correspond power spectra (b) and (d) illustrate the attenuation of higher frequencies from deformed material.	66 ing
28.	The correlation of sample strain with the measured values calculated following the SFPA method. The data points are fitted with the least squares method. The linear data fitting line parameters are $y = 0.0068x + 0.8652$ ; $R^2 = 0.9547$ .	68
29.	Representative steps of quantification using the PSFM method.  (a) selected EBSP 256 x 256 pixel area masked with Hanning window function (b) 2-D Fourier transform of the area in (a),  (c) 1-D averaged at each radiuss 2-D PS in (b),  (d) weighted PS formed from (c) by multiplying each coefficient by its radiuss (A2 = area under PS in (d)).	
30.	The correlation of sample strain with the measured values calculated following the PSFM method. The data points are fitted with	71

#### **KEY TO SYMBOLS AND ABBREVIATIONS**

Å : angstrom, 10<sup>-10</sup> meters
ADC : analog-to-digital converter

b : one byte = eight bits

B : brightness

BSE : backscattered electron coefficient

C : contrast

d : spatial detection limit
D : dimension, e.g., 1-D, 2-D

dc : direct current
E : accelerating voltage

EBSP : electron back scattered patterns
EDM : electric discharge machine

f(x, y): input image function of statistical nature

fcc : face centered cubic FG film : fine grain film

ftp : file transfer protocol

: fourier transform (FFT : fast fourier transform)

g (x, y) : degraded image

G: gain

H : degradation process operator

l : length
m : median
ml : mililiters

 $\begin{array}{lll} \mu m & : \mbox{ micrometer, } 10^{-6} \mbox{ meters} \\ nm & : \mbox{ nanometer, } 10^{-9} \mbox{ meters} \\ n & : \mbox{ mumber of neighbors} \\ \eta \left( x, \, y \right) & : \mbox{ additive noise term} \end{array}$ 

p : pixel P : period

PC : personal computer PS : Power spectrum

PVC plastic : polyvinyl chloride plastic PSFM : power spectra first moment

S,  $\Delta$ S : signal; change in signal due to contrast

SEM : scanning electron microscopy, scanning electron microscope

SFPA : spectral first peak area

V : volts t : time

T (k) : transfer function
w(x) : window function
x : spatial variable
X : abstract variable
Z : atomic number

#### INTRODUCTION

Among various different practical applications where the measurement of plastic strain of materials at the micron-scale can be used, one particular method involves metals reinforced with particles of high stiffness and strength. The distribution of plastic deformation can be measured experimentally using electron back scatter patterns (EBSPs) by quantifying the increased pattern diffuseness with increased strain, which arises as a consequence of the deformation raised dislocation density.

The EBSP technique, introduced by Venables *et al.* in 1973 [1, 2], can be used on bulk specimens and has excellent minimal spatial resolution of approximately 20 x 80 (nm). The technique can be used for local crystallography measurements [3] and phase identification [4]. The growing interest in EBSP is driven by its applicability to local texture measurements of industrial metal alloys [5, 6]. The application of the technique to the analysis of plastic strain (which leads to an increase of the EBSP-pattern diffuseness) was reported by Wilkinson and Dingley [7, 8]. The diffuseness in an EBSP arises from electrons being scattered away from the Bragg condition by dislocations and other defects, which cause a local bending of the lattice planes. Elastic strain measurements in Si<sub>1-x</sub>Ge<sub>x</sub> with micron resolution using EBSP in a scanning electron microscope (SEM) have also been reported [9]. These studies measure the shift of higher-order bands applying a cross-correlation operation. The application of this promising technique has been limited by the

absence of a general and widely agreed method of measuring the pattern quality.

Similarly, there is no general set procedure for obtaining good quality patterns. The procedures vary accordingly to the problems set forward.

This thesis is concerned with determination of the relationship between the microscale deformation of strained bulk materials (primarily Al) and their EBSPs. In this study, the best approaches to evaluate microscale plastic strain deformation of bulk material samples at the micron-scale are determined. Another very important goal is to review the requirements to obtain good quality EBSPs with the facilities available at the Department of Materials Science and Mechanics and elsewhere within the MSU campus. The approach laid out in this thesis originates from the premise that if one can obtain good quality EBSPs from polycrystalline Al, which has low backscattering coefficient, then, with thorough attention to the sample preparation, comparable quality EBSPs should be obtainable from materials with larger atomic numbers, Z. Thus, the material of interest was 99.999% purity Al (Z = 13, fcc,  $a_0 = 4.0497$ Å [10]), which was deformed in compression to four different permanent set strains (0-20%).

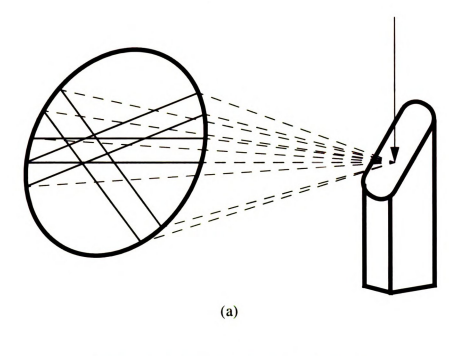
Two original experimental configurations that include signal and image processing stages are described in the thesis. One configuration allows the comparison of the patterns qualitatively, but in real-time, using a video camera; the other does not work in real-time, but has the advantage of acquiring very high quality EBSPs for semi-quantitative measurements, using a remotely controlled photo camera body. The thesis also contains a concise review on the basic physics of acquiring good quality patterns, and describes the experimental setup and procedure for image enhancement and processing.

#### LITERATURE REVIEW

#### 1.1. Use of the EBSP method

The EBSP method allows the measurement of bulk, crystalline or polycrystalline material strain at the micron-scale. The method is based on positioning the electron beam of the scanning electron microcopy (SEM) as a stationary probe on a point on the crystal surface and recording the resulting backscattered electron formed backscattered diffraction patterns as shown in Figure 1. The patterns yield information from a less than 100 nm thick surface layer of a bulk sample and thus the surface conditions and sample preparation are of paramount importance [11]. The backscattered electrons form patterns which contain physical information about the state of the beam-sample interaction volume. The exact volume is determined by the actual electron probe geometry and the accelerating voltage as well as material properties. Spatial resolution volumes as small as 20 x 80 nm for 30 kV primary electron energy and an information depth of the order of 10nm have been reported [1, 2]. A later study [8] suggests a somewhat higher volume of information (200nm diameter, 50 nm depth). For backscattered electrons, the pattern information volume in silicon was evaluated to be of the order of 1µm in diameter [11].

The formation of EBSPs in a scanning electron microscope depends on the diffraction of electrons by atomic planes in the sample, so the distribution, intensity and orientation of the bands forming an EBSP yield information about the crystallography and orientation of the crystal lattice in the sample. Similar information can be obtained using transmission electron microscopy (TEM), but this approach requires relatively complicated sample preparation. Another drawback to TEM is that the area of the sample



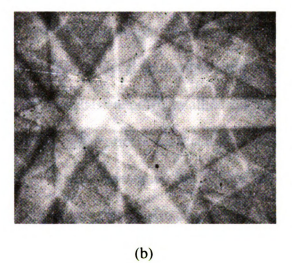


Figure 1. EBSP formation

- (a) illustration of the set up to produce images,
- (b) an EBSP pattern with the first and higher order lines present.

examined is small and not always representative of the bulk material. The crystallography of bulk materials is usually studied using X-ray diffraction, where relatively large sample volumes are needed, but this technique results in the measurement of average properties over a relatively large volume. Thus, SEM, in conjunction with EBSP, fills the gap between the large sample volumes needed for X-ray diffraction and thin foil transmission electron diffraction. Also, sample preparation for EBSP is less critical than that for TEM. For example, patterns can be collected from fracture surfaces.

The EBSP technique introduced by Venables et al. in 1973 [1,2] has also been used for local crystallography measurements and phase identification [3, 4]. The application of electron back scatter diffraction has been extended to the determination of crystal symmetry elements, point groups and space groups [4]. The growing interest in EBSP is primarily driven by its applicability to local texture measurements of industrial metal alloys [5, 6]. Most common materials are polycrystalline aggregates in which the crystal lattice in each individual grains has an orientation that differs from those of its neighbors. The non-random distribution of grain orientation (texture) measurements are used for quality control in materials production [5, 6]. Texture measurements are also important in the understanding of deformation mechanisms.

The application of the EBSP technique to the analyses of plastic strain upon deformation, which leads to an increase of the EBSP pattern diffuseness, was reported by Wilkinson and Dingley [7, 8], where distributions of equivalent plastic strains in an Al6061/ SiC fibre composite measured using the EBSP technique were compared to plastic strain and stress distributions calculated using a continuum mechanics model solved by finite element analysis (FEA). The diffuseness in an EBSP arises from electrons

being scattered away from the Bragg condition by dislocations and other defects, which cause a local bending of the lattice planes. This has the effect of reducing the EBSP quality. It is possible to relate the reduction in pattern quality to the amount of deformation although no overly conclusive results have been obtained as of yet.

Elastic strain measurements with micron level spatial resolution using EBSP on  $Si_{1-x}Ge_x$  thin films have also been reported [9]. In this work, an accuracy of about 0.1% elastic strain was determined from the shift of higher-order EBSP bands applying a cross-correlation operation.

A quantitative theory of EBSPs is based on the many-beam dynamical theory of electron diffraction [12, 13], and assumes that the principal backscattering mechanism is phonon scattering. Even though the theory predicts the main features of patterns, including the bright central band, the usually broad dark first order line, and the sharp light-dark higher order lines, it does not correctly predict the level of the background intensity, particularly for thick crystals.

### 1.2. Physical principles of pattern formation

#### 1.2.1. Amorphous and crystalline samples

If the electron beam strikes an amorphous sample at normal incidence, the angular distribution of backscattered electrons is a cosine function about the surface normal, as shown in Figure 2(a). If the amorphous sample is replaced with a crystal, the general form of the distribution remains the same, but is modulated in magnitude at certain angles, as shown in Figure 2(b). The angles correspond to the Bragg angles of backscattered electrons, diffracted by the lattice, as electrons exit from the lattice [14]. The

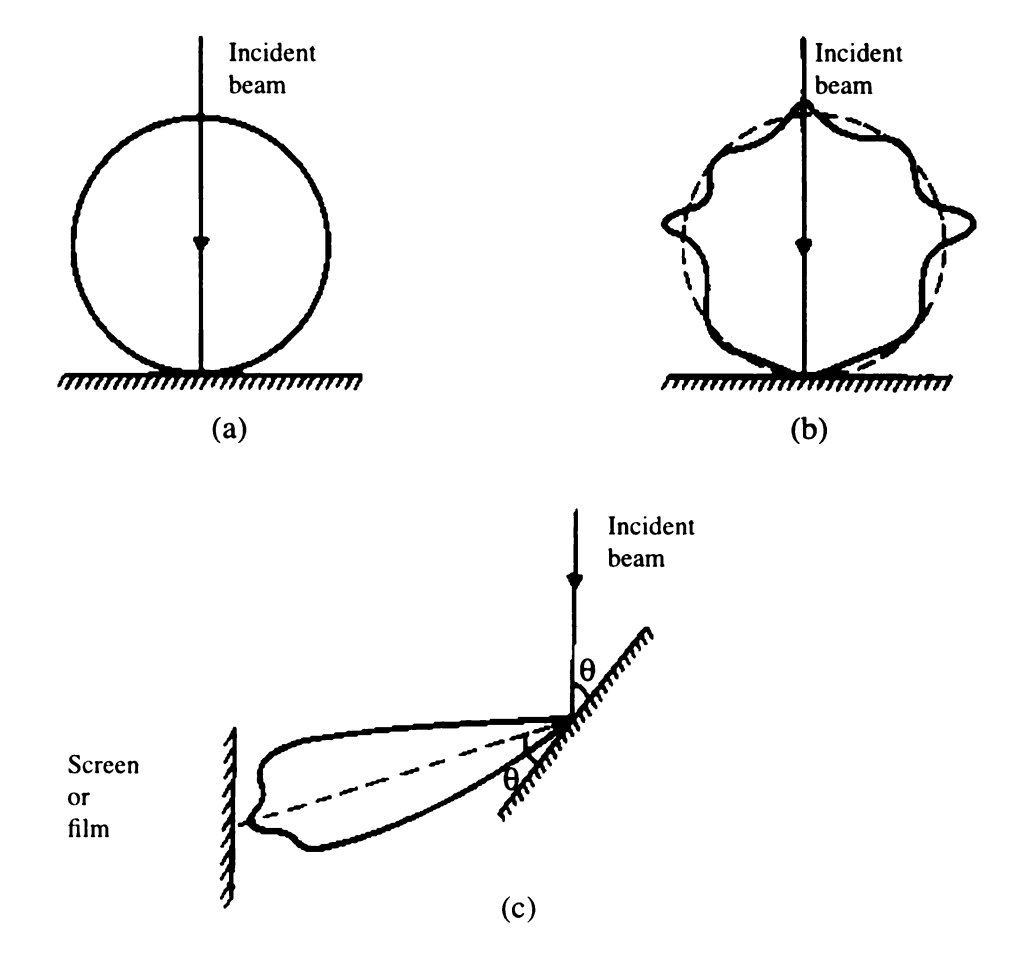


Figure 2. Electron emission profiles (after [11], quoting Laponsky, Whetten, Alam)

- (a) from amorphous materials,
- (b) from crystalline materials,
- (c) the geometry for the production of EBSPs.

backscattered electrons have a wide range of energies and each lattice plane produces a spread of Bragg angles. If the specimen is tilted, as shown in Figure 2(c), the backscattered electrons have energies close to that of the incident beam of electrons [15, 16] in the reflected direction, and the Bragg angles for each set of lattice planes are well defined. Thus, the backscattering coefficient shows modulations at angles related to the symmetry of the lattice of crystalline sample as shown in Figure 1. The backscattered electron coefficient (BSE) is expressed as the ratio of the number of backscattered electrons to the total number of beam electrons incident on the specimen. The BSE is a function of specimen tilt [11, 17], as shown in Figure 3(a). High angles are used for EBSP rendering.

#### 1.2.2. Atomic number and accelerating voltage

In addition to the crystalline nature of a sample and its orientation other variables also affect the physics of pattern formation. For example, the electron backscattered coefficient increases with increasing specimen atomic number, Z, as shown in Figure 3(b), where Monte Carlo calculations [11, 18] are compared with the experimental data [11, 19]. This, in turn, affects the resolution. Electron beams can be focused to nanometer dimensions, which appears to offer an ideal probe and well defined spatial resolution, and can be useful for locating the edge of fine features in a high-density structure.

Unfortunately, the finite size of the interaction volume results in a substantial broadening of the backscattered electron signal profile as the beam is scanned across a grain edge. The study [20] also demonstrated that decreasing the beam energy from 20kV to 5kV produced a substantially sharper rise in the signal profile.

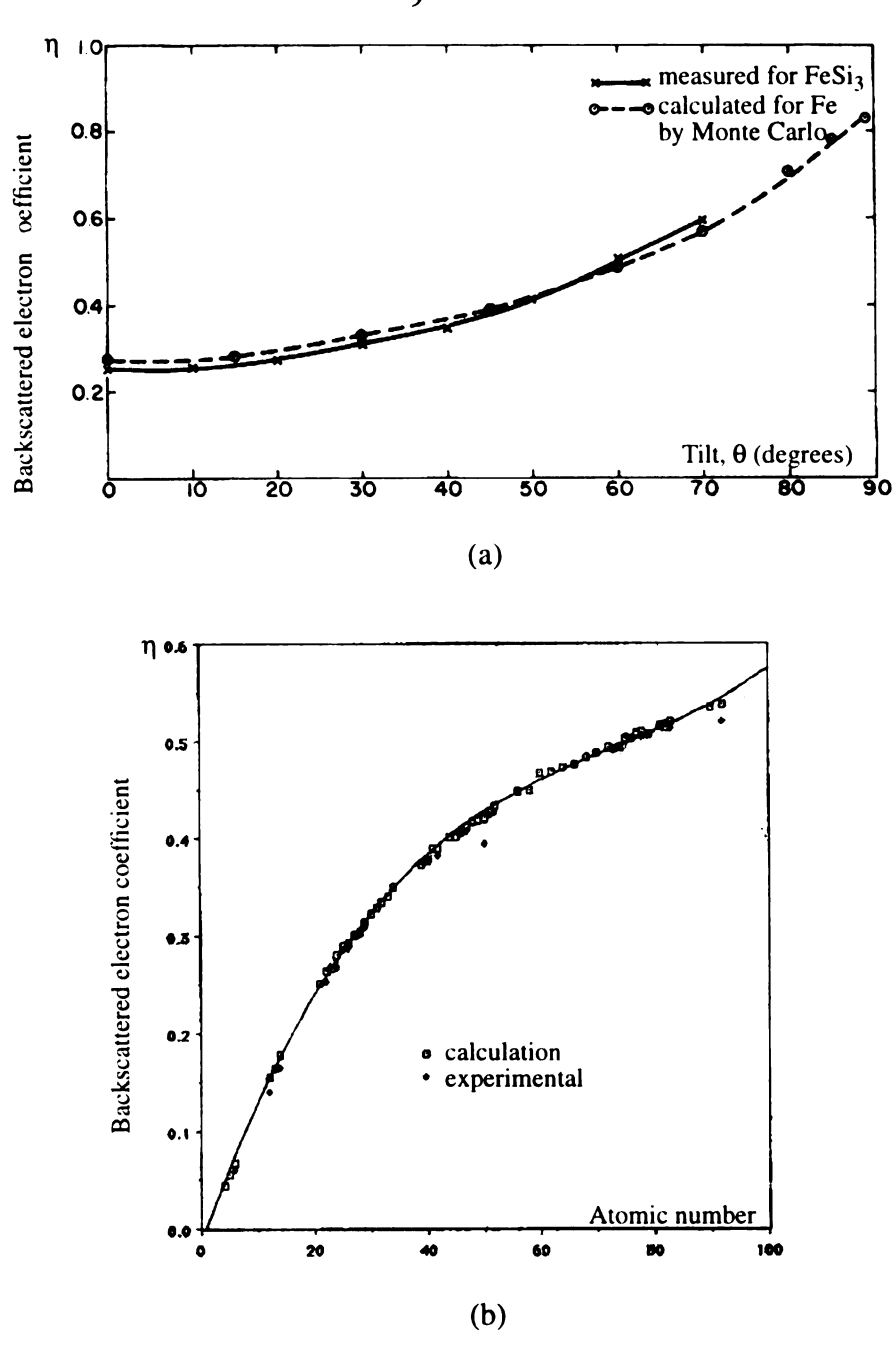


Figure 3. Monte - Carlo simulation predicted effects (after [11], quoting Newbury, Myklebust, Heinrich)

- (a) dependence of the backscattered electron coefficient (BSE) on specimen tilt,
- (b) dependence of the BSE coefficient on the atomic number of the target; E = 20 kV.

#### 1.2.3. Surface preparation

In addition to the microscope condition and bulk nature of the material, the specimen surface condition is critical in forming EBSP images. Generally, a clean specimen is required for application of the EBSP method. Additionally, as the electron beam impinges upon specimen area, A, the latter should be smooth on the scale of the effective interaction volume diameter. The effective interaction volume diameter is of the order of 1  $\mu$ m [2, 8]. The interaction volume size is related to applied accelerating voltage and secondary electron image resolution as well as material properties. The minimal secondary electron image resolution is determined by the electron probe diameter, which is approximately 35Å for the Hitachi S-2500 used in this study. However, the BSE interaction volume is much larger.

Because the contrast primarily comes from a less than 500-1000 Å thick surface layer, the specimen to be observed must have a surface that is both clean, e.g., free from hydrocarbons, oxides, etc., and undamaged. Conventional mechanical means of surface preparation are often unsuitable because they cause chemical contamination and leave plastic damage. The most suitable approach is to chemically or electrochemically polish the material to be observed [11]. Polishing procedures and details can be found in references [11, 20-23]. Before observation, it is desirable to wash the specimen surface with electronic grade ethanol (stored in glass, not in a squeeze bottle) to remove any traces of finger or vacuum grease.

According to Hirsch et al. [21] the transmission of electrons through material increases at lower temperatures. This effect can be explained in terms of the reduced penetration of Bloch waves (the electron regarded as a fixed linear combination of the two

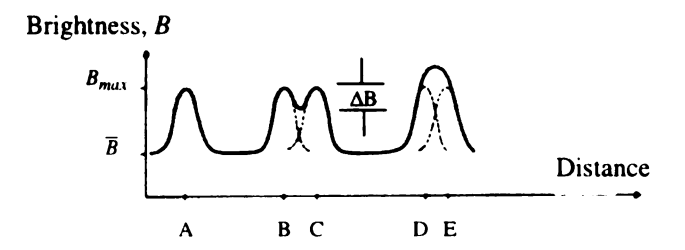
Bloch wave functions) in a vibrating lattice at high temperatures. The Bloch wave functions are the fundamental solutions of the dynamical theory, and each of the two Bloch functions consists of a definite combination of plane waves. The amplitude of atoms' thermal vibrations is smaller at low temperatures. Thus, the temperature around the specimen should be as low as possible; the liquid nitrogen temperature would be ideal.

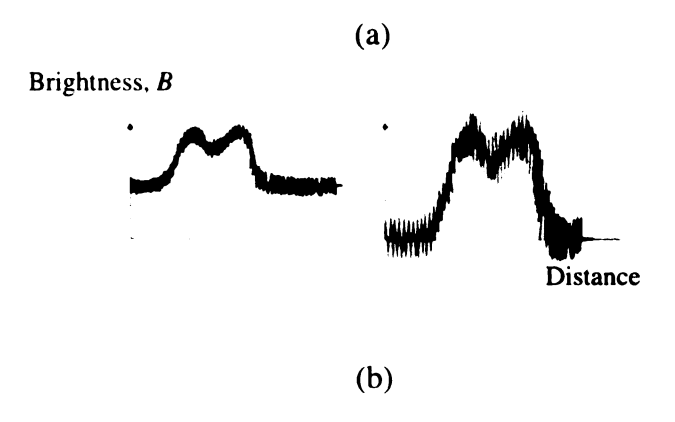
#### 1.3. Digital image enhancement

In this section, some concepts of image processing used in the thesis and implemented by image processing software SEMPER 6.4, which is run on a 486/50 MHz PC in our hardware setup, will be illustrated. A number of different image processing examples will be given as part of this discussion.

#### 1.3.1. LINK digital processing

In the EBSP method, a stationary beam is used to collect data from the smallest possible region. It is important that the backscattered signal is strong enough to produce a visible and recordable image. Using an aberration free electron beam and high electron beam current (filament material is thus very important in EBSP), the bands can be displayed on a fluorescent screen and imaged in real time using a sensitive TV camera. Since the final image point resolution depends on the rendering media contrast (film or phosphor screen) and the signal-to-noise ratio, the use of a phosphor screen limits the resolution as compared to photographic film (due to differences in grain size). The Rayleigh contrast criterion (after [11], quoting Everhart, Leisegang) states that in general two points are resolved if the intensity at the minimum between them is less than 75% of the observed maximum intensity, as shown in Figure 4(a). This limit varies for different





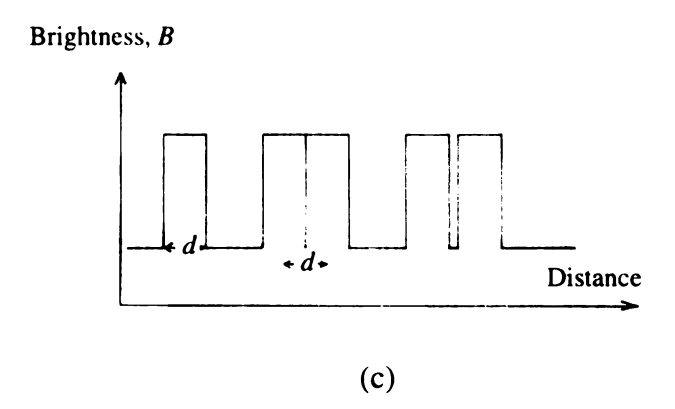


Figure 4. Multimode scanning electron microscopy [11]

- (a) point resolution along a line scan. Two points are resolved when  $B_{max} \Delta B \leq 0.75 \; B_{max} \; \text{or} \; \Delta B \geq 0.25 \; B_{max},$
- (b) signal line scan trace without back-off and with back-off and increased amplifier gain,
- (c) if the spatial detection limit is d and the point brightness peak is of square waveform, the contrast minimum between adjacent bright points rises suddenly.

signal-to-noise ratios (Figure 4(b)). For high noise levels, a fall of 25% will not be reliably detectable and the minimum separation of resolvable points will be increased. Also, the minimum value of the point resolution cannot be less than the spatial detection limit, as shown in Figure 4(c). Like contrast, resolution is degraded by noise. The majority of the contrast is carried by the backscattered electrons whose energy lies closest to the incident beam energy. Experimental and computed data for copper impinged by 20 keV electrons demonstrates that the contrast is only 1.6% when all backscattered electrons are collected, and is in excess of 40% if collection is restricted to backscattered electrons lying within 100 eV of the beam energy, i.e. 19.9 - 20 keV (after [11], quoting Wells, Sandstrom). Because of this fact, alternative backscattered electron detectors exist.

Using the LINK Merlin EBSP Camera System [23] available in the Materials Science and Mechanics Department, the contrast of acquired patterns is too low to provide satisfying visual information. Therefore, the images must be enhanced. This requires the images be converted from the analog form into the digital form with maximum efficiency using as many digital levels as possible. The analog to digital conversion is performed using an analog to digital converter (ADC) and the obtained EBSPs are digitally stored. Even though main pattern details are visible, the captured EBSP images usually are noisy (in our case contrast is approximately 5%). To provide an image that properly displays the details of the pattern, images must be enhanced in some way. Enhancement techniques are procedures which are designed to manipulate an image in order to take advantage of the psychophysical aspects of the human visual system.

#### 1.3.2. Differential signal amplification (contrast expansion)

If the signal has a relatively large "dc-component" (its modulation depth is very small) and its signal is fitted to the range of the analog-to-digital converter, the actual pattern modulation may occupy only a few digitization levels. The solution to this problem is called the differential signal amplification, also known as black level correction or contrast expansion. Most SEMs offer this capability in the form of the contrast control. In this technique [24, 25], the unvarying component of the signal (background level), which contains no information, is subtracted away, and the residual signal is amplified to fill the dynamic range of the display system. By this procedure, the signal contrast can be amplified many times. If the SEM does not have this capability, the signal can be transmitted through an RC-integrator (resistance-capacitance integrator) that holds the average of the signal (RC-time in the order of seconds) and subtracts this average from the actual signal. This difference is then amplified to match the input range of the ADC used. If the ADC takes only positive inputs, some offset is required to lift the ac-signal into the positive domain. This method stipulates that the beam current has to be high enough to ensure an adequate signal-to-noise ratio.

#### 1.3.3. Frame averaging

Because of the random distribution of the events in time, as the number of frames averaged goes up, the signal-to-noise ratio improves. Quantitatively, Rose [26, 27] evaluated the ability of observers to detect contrast between two very small regions in a scanned TV image in the presence of noise, as  $\Delta S > 5N$  (Rose criterion), where  $\Delta S =$  the change in signal due to the contrast, N = noise, as shown in Figure 5. Considering the

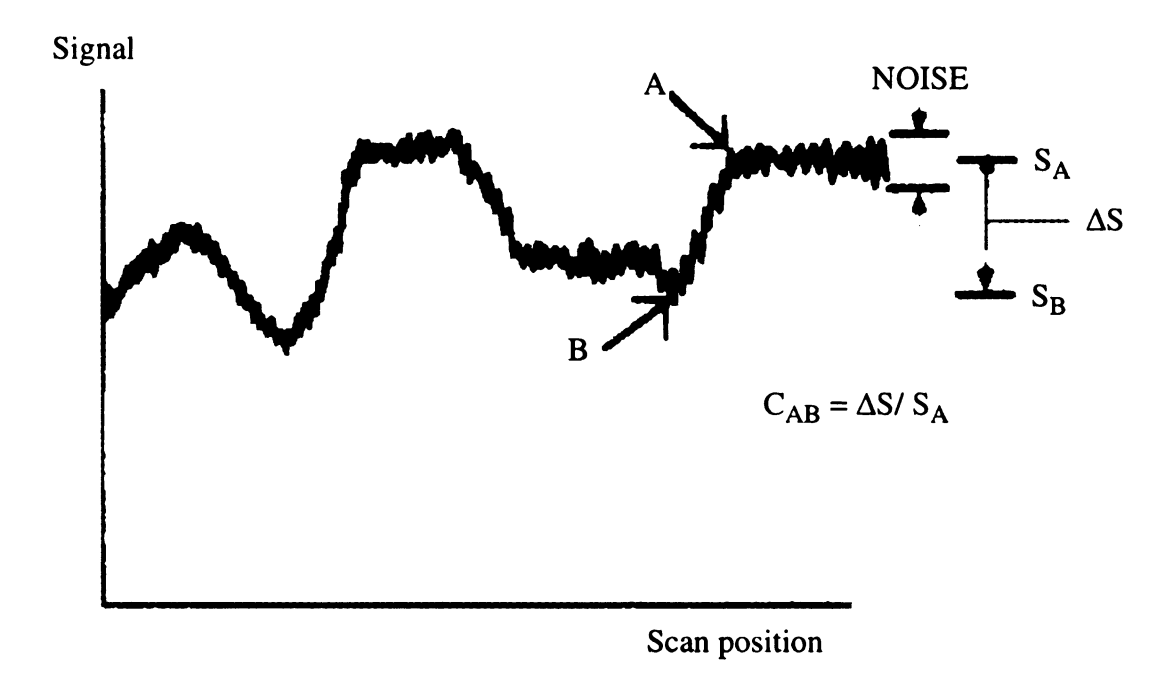


Figure 5. Illustration of a scan line trace across an image. "A" and "B" are two arbitrarily chosen points.

noise in terms of the number of signal events, the equation  $C > 5n^{-1/2}$  was obtained [28]. For example, in order to observe a given level of contrast, say C = 0.0833 = 8.333%, a mean number of signal carriers,  $n > (5/C)^2 = 3600$ , must be collected per picture point. With the TV rate (30 frames/ sec), this can be done by averaging  $\ge 3600/30 = 120$  sec = 2 min. However, the beneficial effects of frame averaging must be balanced in an SEM with the general loss of image quality resulting from beam damage and specimen contamination.

### 1.3.4. Histogram modification

A histogram of the gray-level content of a digitized EBSP pattern provides a global description of the image appearance. A gray-scale image is a graphic that contains more than one bit of information per pixel to convey shades of grey. For example, images that have  $256 = 2^8$  shades of grey and require 8 bits = 1 byte (1b) per pixel were used in the present study. An average image consists of  $768 \times 512$  pixels, and as a result is at least  $16 \times 768 \times 512 = 383$ Kb  $\cong 0.4$ Mb in size.

Several image modification methods based on histograms exist [16, 28]. One of them is histogram thresholding and stretching. That is, assigning the darkest desirable pixels in an image to pure black (0) and the brightest desirable pixels to full white (255), with intermediate intensities being linearly varied between these extremes. This operation allows the full utilization of the available intensity range of the display system (256 for our system). Histogram thresholding and stretching is a very important and easy method to visually optimize images. The histogram-equalization/ normalization technique increases the dynamic range of the pixels by obtaining a quasi-uniform density histogram

throughout the full range of gray levels from a histogram with a narrow ranges of values (a large and narrow peak). To accomplish normalization, the transfer function:  $T(k) = 1/T \sum_{i} n_i$ , for k = 0, ..., 255 is used. The result of this transfer function is a new image and histogram, with the pixel intensities distributed as evenly as possible. If the original histogram was a continuous mathematical curve, then T(k) would be its integral. The result of image normalizing is shown in Figure 6. When it is necessary to highlight certain gray-level ranges in an image, the direct histogram-specification method can be used, as shown in Figure 7.

# 1.3.5. Spatial-domain techniques (averaging, median filtering, background subtraction)

"Neighborhood averaging" averages the value of a particular pixel from the values of the closest (neinghbor) pixels. This technique is used for image smoothing [28]. However, while the method decreases noise, it also produces a blurring effect proportional to the size of neighborhood used. Over many pixels, say 40 x 40, avaraged image is similar to the image background (the dc component), because this operation integrates out sharp details - the ac component, including also peaks and spikes, as shown in Figure 8.

The sharp detail can be maintained and the edge blurring circumvented in two ways. First, pixels with certain values can be cut off, or a threshold may be used. Alternatively, median filters may be used. While in median filtering, the gray levels of a pixel are replaced by the median value of the gray levels in a neighborhood of that pixel, instead of by the average. The median, m, of a set of values is such that half of the values in the set are less than m and half are greater than m.

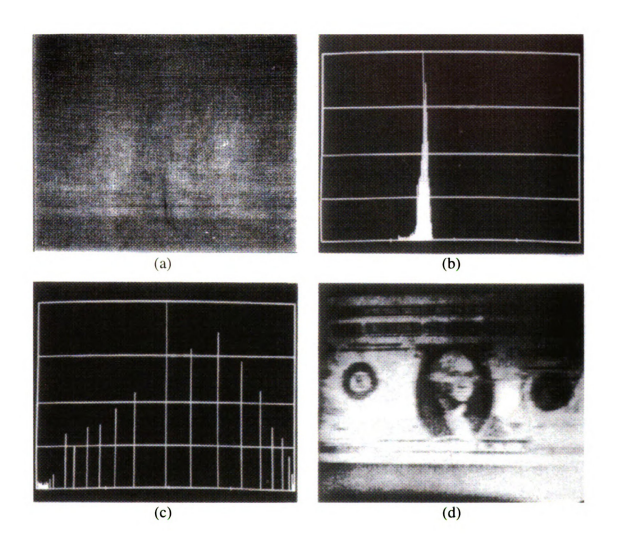


Figure 6. Illustration of the histogram-equalization approach [28]

- (a) original image,
- (b) original histogram,
- (c) equalized histogram,
- (d) enhanced image.

19

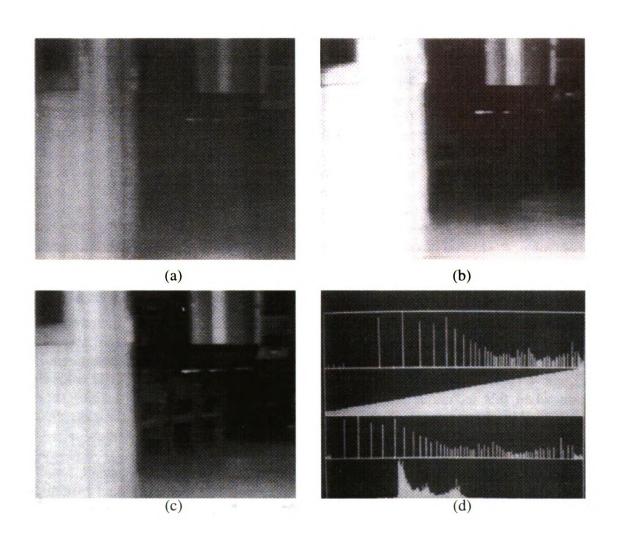


Figure 7. Illustration of the histogram-specification method [28]

- (a) original image,
- (b) histogram equalized image,
- (c) image enhanced by histogram specification,
- (d) histograms.



Figure 8. Image smoothing by averaging and median filtering [28]

- (a) original image,
- (b) image corrupted by impulse noise,
- (c,d) result of 5 x 5 neighborhood averaging, and 5 x 5 median filtering of the corrupted image.

Background subtraction is performed on an averaged image by subtracting the experimental background [29] or, alternatively, subtracting the theoretical (calculated) background obtained from statistical 3-D considerations. Successful subtraction can greatly enhance the contrast of the pattern. The theoretical background can be calculated from the original pattern by application of a local-mean (or, alternatively, median) operation over 40 x 40 neighboring pixels [30].

### 1.3.6. Frequency-domain methods

Image smoothing (low-pass filters) is based on the fact that edges and other sharp transitions (such as noise) in the gray levels of an image contribute heavily to the high-frequency content of its Fourier transform. It follows that the noise can be decreased by attenuating a specified range of high-frequency components in the transform of a given image [28]. When high-frequency components are filtered out and information in the low-frequency range is passed without attenuation, the method is called lowpass filtering. Results applying ideal lowpass filters with different cut-off frequencies, are shown in Figure 9. The blurring in Figure 9(c) is an indication that most of the edge information is contained within the 10% power removed by the filter (outside the 2-D Fourier spectrum). Lowpass filtering reduces spurious effects at the expense of image sharpness.

Image sharpening (differentiation, highpass filtering) techniques are useful as image enhancement tools (Figure 10). The differentiation sharpens a given image. The most commonly used method of differentiation is the gradient. Since edges and other abrupt changes in gray levels are associated with high-frequency components, image sharpening can be achieved in the frequency domain by a highpass filtering process.

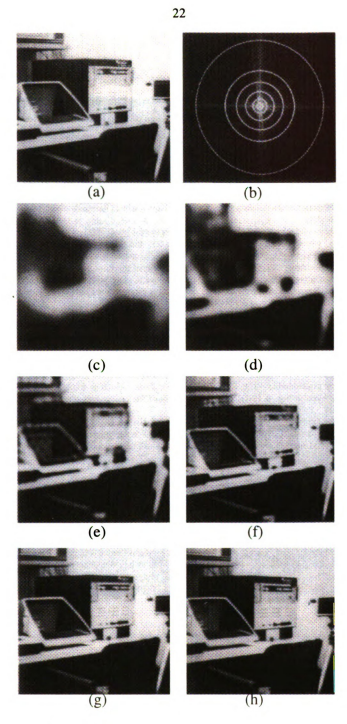


Figure 9. Lowpass filters [28]

- (a) 256 x 256 pixel image,
- (b) its 2-D Fourier spectrum. The superimposed circles, which have radii equal to
- 5, 11, 22, 36, 53, and 98 enclose 90, 95, 98, 99, 99.5, and 99.9% of the image power,
- (c-h) results of applying ideal lowpass filters to (a). The radii 5-98 correspond to c-h.

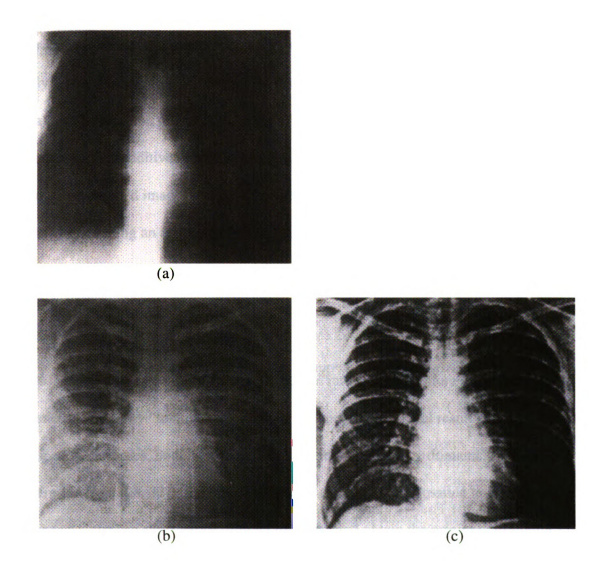


Figure 10. Example of highpass filtering [28]

- (a) original image,
- (b) result of high-frequency emphasis, i.e., highpass filtering,
- (c) high-frequency emphasis and histogram equalization.

### 1.3.7. Image restoration

Image restoration is a process that attempts to reconstruct an image that has been degraded. The restoration techniques are oriented toward modelling the degradation and applying the inverse process in order to recover the original image. As shown in Figure 11(a), the degradation process can be modelled as a system (or operator), H, which together with an additive noise term,  $\eta(x, y)$ , operates on an input image, f(x, y), to produce a degraded image, g(x, y). The digital image-restoration problem may be viewed as that of obtaining an approximation to f(x, y), given g(x, y) and the degradation in the form of the operator, H. It is assumed that our knowledge about  $\eta(x, y)$  is limited to information of a statistical nature [27].

#### 1.3.7.1. Interactive restoration

It is possible to take advantage of human intuition and restore the images in an interactive mode, by "tuning" the available parameters. The final result may be adequate for specific purposes, both in spatial, as well as in the frequency domains, as shown in Figure 11 (from [28, 32]). Figure 12 illustrates that when it is possible to identify the noise term, one can satisfactory subtract the noise and obtain the original. In Figure 11(b-d), the noise term is identified in 2-D Fourier space. One goal of this study is to determine if any periodic signal can be identified and processed using the 2-D Fourier spectrum.

### 1.3.7.2. Restoration in the spatial domain

Figure 12 [28, 33] shows an infrared image corrupted by quasi-periodic scanner interference, visible as a "ripple" effect in the vertical direction. Because of its periodic nature, the interference produces bursts of concentrated energy in the vertical axis of the Fourier spectrum of the image (Figure 13(b)). The effect of interference can be reduced

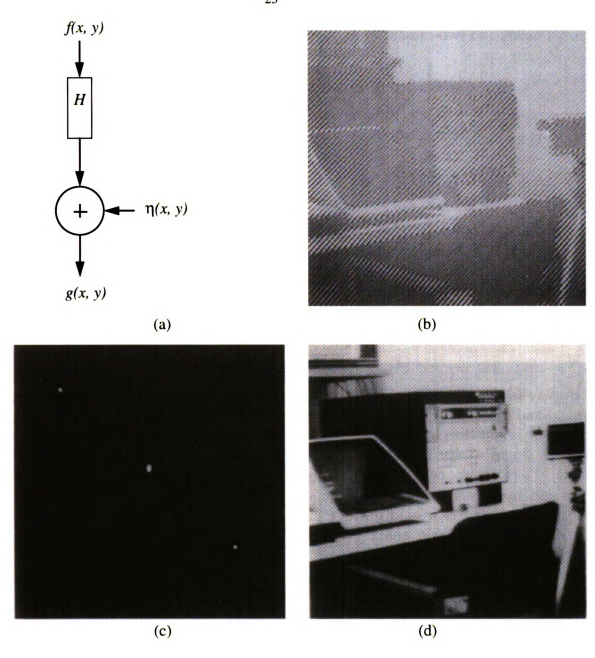


Figure 11. Example of interactive restoration by sinusoidal interference removal [28] showing

- (a) a model of the image degradation process,
- (b) a corrupted image,
- (c) a Fourier spectrum showing impulses due to sinusoidal pattern, and
- (d) an image restored by using a band-reject filter with a constant radius.

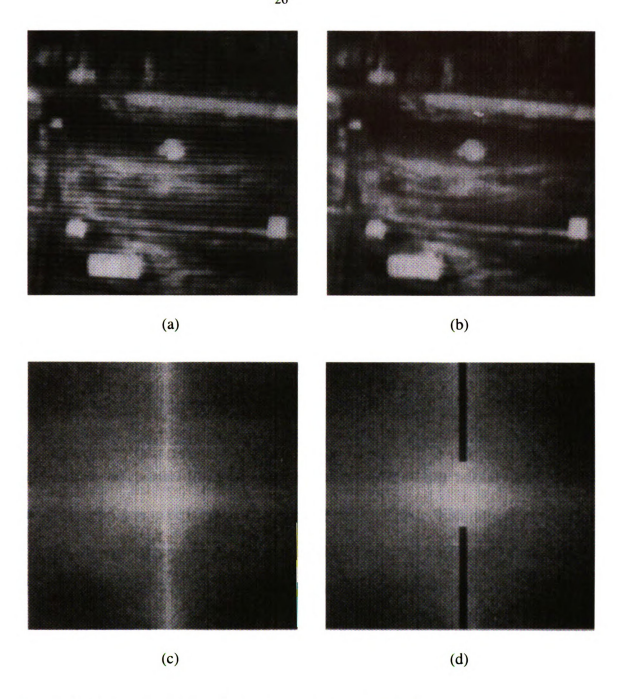


Figure 12. Restoration in the spatial domain [28] demonstrating

- (a) an infrared image showing interference,
- (b) an image restored using a notch filter in the frequency domain,
- (c) a Fourier spectrum of the image in (a), and
- (d) a notch filter superimposed on the spectrum.

by using a notch filter, H(u, v), which attenuates the values of the Fourier transform in the vertical axis and multiplies all other values of the transform by 1 (dark bands are the attenuated regions). The image restoration uses extensive computation time and may or may not give correct profiles of the EBSP bands. Thus, it is the last resort to obtain satisfactory images. In simple terms, if one knows or can intelligently guess what the noise term/input image functions or their Fourier spectra look like, there is a chance to restore or improve the input image.

# 1.4. EBSPs quantification mathematical aspects

Only after the image is satisfactory and images from different samples can be enhanced in the same standardized way, can the quantification of EBSPs be attempted. One particular application of interest is the measuring of the distribution of plastic deformation. To compare EBSPs from different samples, the EBSP lines around a particular zone have to be taken as a common feature [7, 8, 34]. With increasing strain, EBSP diffusiveness increases, meaning attenuation of higher order Fourier components. Thus increases in EBSPs diffusiveness can be measured in Fourier space.

The essence of the Fourier transform of a waveform involves the decomposition of the waveform into a sum of sinusoids of different frequencies, as illustrated in Figure 13(a). The power spectrum, the squared modulus (intensity) of a Fourier transform, is used for detecting and measuring periodic features [35]. The power spectrum, like any other function f(x), can be characterized by its first moment. By analogy with mass distribution along a line, the first moment of f(x) about the origin is defined as  $\sum x f(x)$  for a discrete f(x). For a simple case of an impulse pair in which each impulse has a

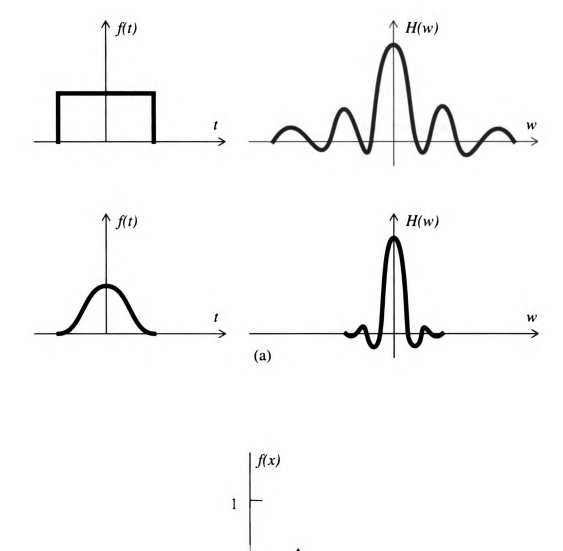


Figure 13. Fourier transform properties (after [35, 36])

- (a) Fourier transform pairs show the emphasis of the Fourier transform central peak as the original changes from the rectangular to the more "diffuse" bell-shape form,
- (b) the first moment,  $\sum x f(x)$ , characterize function's f(x) distribution along a line. The impulse pair's first moment is  $1/2 = (-1/2) \times (-1/2) + 1/2 \times 1/2$ .

(b)

positive moment  $1/4 = 1/2 \times 1/2$ , the total first moment is 1/2 = 1/4 + 1/4 (Figure 13(b))

[36]. Extending this approach, the *n*th moment  $m_n$  of f(X) is  $m_n = \int t^n f(X) dX$ , n = 0,1, [37].

EBSPs can be analyzed in two domains: the spatial domain and the frequency domain. In the spatial domain, two single-valued parameters, the spatial mean (the dc component, or a spatial average of the f(x) signal) and the temporal root mean square (spatial average of  $f^{2}(x)$ ) are used to describe a signal. In the frequency domain, the data is represented as a function of frequency,  $\omega$ . To store and use the real data, the waveform information has to be sampled. Processing of an analog signal involves multiplication of the signal by both a window function w(x) with length, l, and a sample function, s(x), that selects the points to be digitized. The original analog signal is represented by the digital sequence of equally spaced numbers. The discrete frequency components are processed to yield discrete periodic frequency components, transient continuous spectrum frequency components, and random mean square (power) spectral density frequency components. To avoid aliasing [34], or the distortion of the desired Fourier transform of a sampled function, the sample interval should be sufficiently small. The sampling interval limits the highest frequency component of the Fourier transform that can be obtained without the aliasing.

The truncation at a position other than a multiple of the period, P, creates a periodic function with sharp discontinuities. In the frequency domain, this introduces additional higher frequency components termed leakage. To reduce leakage, it is necessary to use special windowing or truncation functions. An ideal filter acts like a Dirac delta function, but it is not practical to implement such a filter in the spatial domain. The transmission characteristics of a practical filter are described by four parameters in the

frequency domain: center frequency, bandwidth, ripple, and selectivity (Figure 14(a) [38]). It is often advantageous to look at the Fourier transforms of the windowing functions to analyze what their response is. The four most commonly employed window functions are rectangular, Hanning, Kaiser-Bessel, and flat-top, as shown in Figure 14(b). The window center is emphasized. The selectivity in separating closely spaced frequency components with widely varying amplitudes varies for each window function (Figure 14). Selection of the windowing function is generally a compromise between the width of the central peak (which one wants to be as small as possible) and the height of the side lobes (which are also wanted as small as possible). In the present study, the Hanning window was selected, because it works well in EBSP applications [39] and is a good general purpose filter for both periodic signals and random signals. The function brings intensities down to zero at edges quite steadily, and also brings the intensity gradient to zero.

The central peak height in the power spectrum reflects the mean intensity level in the original image. This is an important point to understand since it will affect many parameters that could be formed from the power spectrum. Before calculating the power spectrum, the mean intensity level in the image should be set to zero (after any windowing) [39]. This should be done for both 1-D and 2-D cases. By doing this, the power spectrum is prevented from being swamped by a very large central (zero frequency) spike, which will get larger in proportion to the mean intensity in the image. The parameters that could be developed to characterize images only work well if the images to be compared hold the same basic information, albeit more "blurred" than in others. That is, the EBSP patterns to be compared must contain the same crystallographic region, for example the region near a <112> zone.

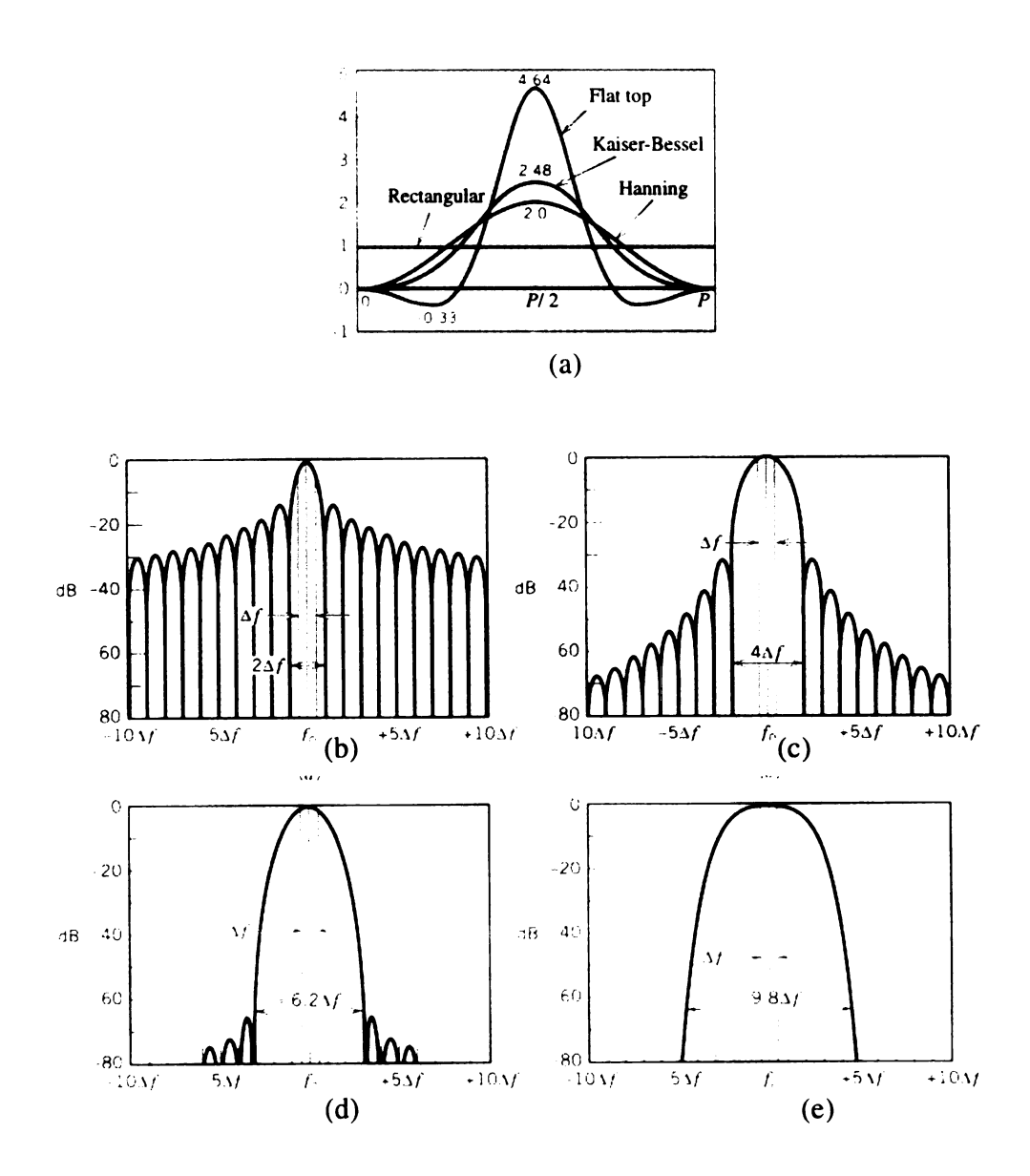


Figure 14. Digital filter characteristics
(after [34], quoting Bruel and Kjaer Instruments)
(a) graphic displays of four common window functions
(rectangular, Hanning, Kaiser-Bessel, and flat-top) in the time domain.
The area under each window function is unity,

(b-e) filter shapes for weighting with (b) rectangular, (c) Hanning,

(d) Kaiser-Bessel, (e) flat-top window functions.

In summary, after careful sample preparation, electron backscattered patterns can be obtained from almost any material. A noise component is an inherent part of electron back scattered patterns. The signal-to-noise ratio can be increased by signal enhancing operations. Different signal processing operations are essential to improve the appearance of the images and to make the patterns suitable for quantification.

In the present work, sample preparation and image processing techniques will be optimized for two approaches for EBSP acquisition. Enhanced images will be used to demonstrate the feasibility of using EBSP for microscale plastic strain quantification.

#### EXPERIMENTAL PROCEDURE

### 2.1. Sample deformation

The formation of EBSPs depends on the diffraction of electrons by atomic planes in the sample. Therefore, the distribution, intensity and orientation of the bands forming the EBSP yield information about the crystallography and orientation of the crystal lattice of the sample. The diffuseness in an EBSP arises from electrons being scattered away from the Bragg condition by dislocations and other defects, which cause a local bending of the lattice planes. This has the effect of reducing the EBSP quality. Therefore, in order to properly quantify EBSPs, it is necessary to avoid any deformation artifacts and, thus, the sample preparation is very important.

The material used in this study was a 99.999% purity aluminum bar provided by Dr. D.A. Grange, Alcoa Technical Center. A large number of smaller rectangular cubic test pieces (1 x 0.5 x 0.5 (cm)) were machined from the bar by blade cutting and sanded with silicon carbon metallographic paper.

All of the samples were annealed under the same conditions to ensure reproducibility. A servohydraulic 810 Materials Testing System<sup>TM</sup> with a vacuum furnace was used for both vacuum annealing and subsequent compression runs. The samples were annealed for two hours at 400 °C in 7 x 10<sup>-6</sup> torr vacuum. Approximately twenty samples were clamped together and put on the platform at the same time. By having a good thermal contact between the samples, thermal differences across the platform were minimized, at the same time ensuring that annealing was time efficient.

The samples were deformed in compression in air at ambient temperature to a

number of different permanent set strains in the interval between 0 - 20%. The goal was to get samples whose actual deformations were somewhat uniformly distributed in the 0 - 20% range. The constant crosshead displacement technique was used. The actual deformation was determined by measuring the sample dimensions with calipers before and after the compression process. The Materials Test System<sup>TM</sup> allows for the setting of experimental deformation parameters, such as strain, and thus is convenient to use. Yet, because of factors such as elastic sample spring-back and compliance in the machine (platens, hydraulic drive rods), the set deformation values are higher than the actual final deformation of samples. This difference increases with increasing deformation and must be taken into account. A number of compression strain values were targeted and the actual strain values obtained were calculated.

The actual uniform compression procedure and the desired deformation value were set in the Material Test System<sup>TM</sup>. Because the same standard strain rate  $10^{-3}$  strain/s (= 0.1% strain/sec) was desired for all the samples, the desired strain rate was to be translated into crosshead displacement rate and compression rate in percents of full scale of the machine strain range. After calculations, the compression rate value for the machine used was found to equal  $l \times 10^{-2}$ . Two important specific unit values of the Materials Testing System<sup>TM</sup> were 1 time unit = 1 sec, 100% range = 10 mm.

From approximately twenty annealed and deformed samples, four were chosen for subsequent sample preparation and EBSPs quantitative measurements. The strain values selected were 0%, 5.4%; 14.7%, 18.3%.

After a surface preparation procedure, explained in details in the next section, the average grain size was evaluated using optical microscopy. The annealed 99.999% pure

polycrystalline Al grain diameter size, measured with a scaled eye piece in a Leco optical microscope, was found to be approximately 1 to 2 mm.

## 2.2. Surface preparation

For application of the EBSP method, the sample preparation must produce a sample surface which is smooth and clean. Also, the EBSP sample preparation must avoid introducing plastic deformation in the surface adjacent layer. The specimen should be smooth on a scale of the effective interaction volume diameter, d, which is of the order of 1  $\mu$ m [2,8]. The effective interaction volume diameter decreases as the applied accelerating voltage becomes smaller.

The specimen must also have a surface that is free from hydrocarbons, oxides, and other contaminants. The surface layer lattice should be undamaged and ordered (crystalline or polycrystalline). Because EBSPs blur as a result of surface layer deformation, the layer's lattice should not be deformed or disordered (amorphous) beyond the method's sensitivity threshold. Conventional mechanical means of surface preparation are often unsuitable because they cause chemical contamination and leave plastic damage. The most suitable approach is to chemically or electrochemically polish the crystal to be observed [11].

As sample preparation is very important, it takes both time and considerable experimental effort to determine the best sample preparation technique for a particular sample material. Because of this, the EBSP method is sometimes referred to as a semi-quantitative method. The optimum Al sample mechanical grinding and electropolishing preparation procedures used in this study were developed by Mr. A.W. Gibson during his

master's project [40] initial investigation. Mr. Gibson tried multiple different intermediate mechanical, and final sample preparation chemical and electro-chemical polishing methods, and showed that changes in sample preparation technique directly affects the EBSP quality. The quality changed from the point of hardly distinguishable EBSPs bands to well defined EBSP bands on which quantitative measurements can be undertaken.

The standard EBSP bulk Al sample preparation used in this study includes three important stages:

- cutting the annealed and mechanically deformed polycrystalline Al bulk samples to obtain rectangular samples. For convenience in the present study, an extra step was performed that is not necessary for general EBSP work. Namely, the rectangular samples were cut in half with a diamond saw. This enables one to access a representative, average sample volume, and also double the sample surface area accessible with EBSP method,
- smoothing the faces by mechanical polishing of the cut surface,
- removing the traces of worked metal using a final electrochemical polish.

In this study, a Struers Accutom-5<sup>TM</sup> microprocessor controlled cut-off machine was used. The cut-off machine is equipped with a high-precision stepper motor enabling positioning in steps of 5 μm. The feed speed can be controlled from 0.005 to 3.00 mm/ sec. The Accutom-5<sup>TM</sup> has a variable wheel revolution speed of up to 3000 rpm. For soft and medium soft metals with hardness HV 30-350 the machine's manual [41] recommends medium force limit, feed speed between 0.05 - 0.30 mm/s, and the wheel speed 1000 - 3000 rpm. To obtain low wheel wear and better surface quality, it is recommended to always use the highest wheel speed. For cutting the Al material samples,

3000 rpm wheel speed, 0.075 mm/s wheel speed and a diamond cut-off wheel were used.

Several sample preparation methods were evaluated in order to determine the best approach for obtaining optimum EBSP images. The goal was to find the cutting technique that cuts without introducing deformation in the surface adjacent layer, and, at the same time, is not too slow. Electro discharge machining, diamond wafering cutting, and acid saw cutting techniques were considered. Saws for the first two cutting techniques are located at the Department of Materials Science and Mechanics, while an acid saw is available at the Department of Physics. The results are summarized in the section 3.3.

After the sample is cut, the next step is mechanical polishing. A good reference for, and a description of metallographic polishing techniques is a book by Samuels [42]. Softer alloys generally are more difficult to prepare by mechanical polishing because

- deformation caused by cutting and grinding extends to a greater depth,
- the embedding of abrasive particles in the metal during polishing is more likely.

Silicon carbide sand papers (240-C, 320-C, 400-C, and 600-C grit) was used for grinding. Then, using LECO Corporation VARI/ POL VP-150<sup>TM</sup> polishing wheels run at 300 rpm, the samples were mechanically polished with 5  $\mu$ m and 0.3  $\mu$ m Al<sub>2</sub>O<sub>3</sub> suspensions, monitoring the polish appearance with an optical microscope.

Since this surface preparation technique introduces a deformed surface layer [42] into the specimen, electropolishing was used to quickly remove this surface damage [43]. Electropolishing is controlled by the electrolyte temperature, stirring rate, applied voltage and resulting current, and by the orientation of the specimen. By varying the applied voltage before starting the electropolishing, the optimum working voltage was determined to be 20V (Figure 15). Working at this voltage avoided:

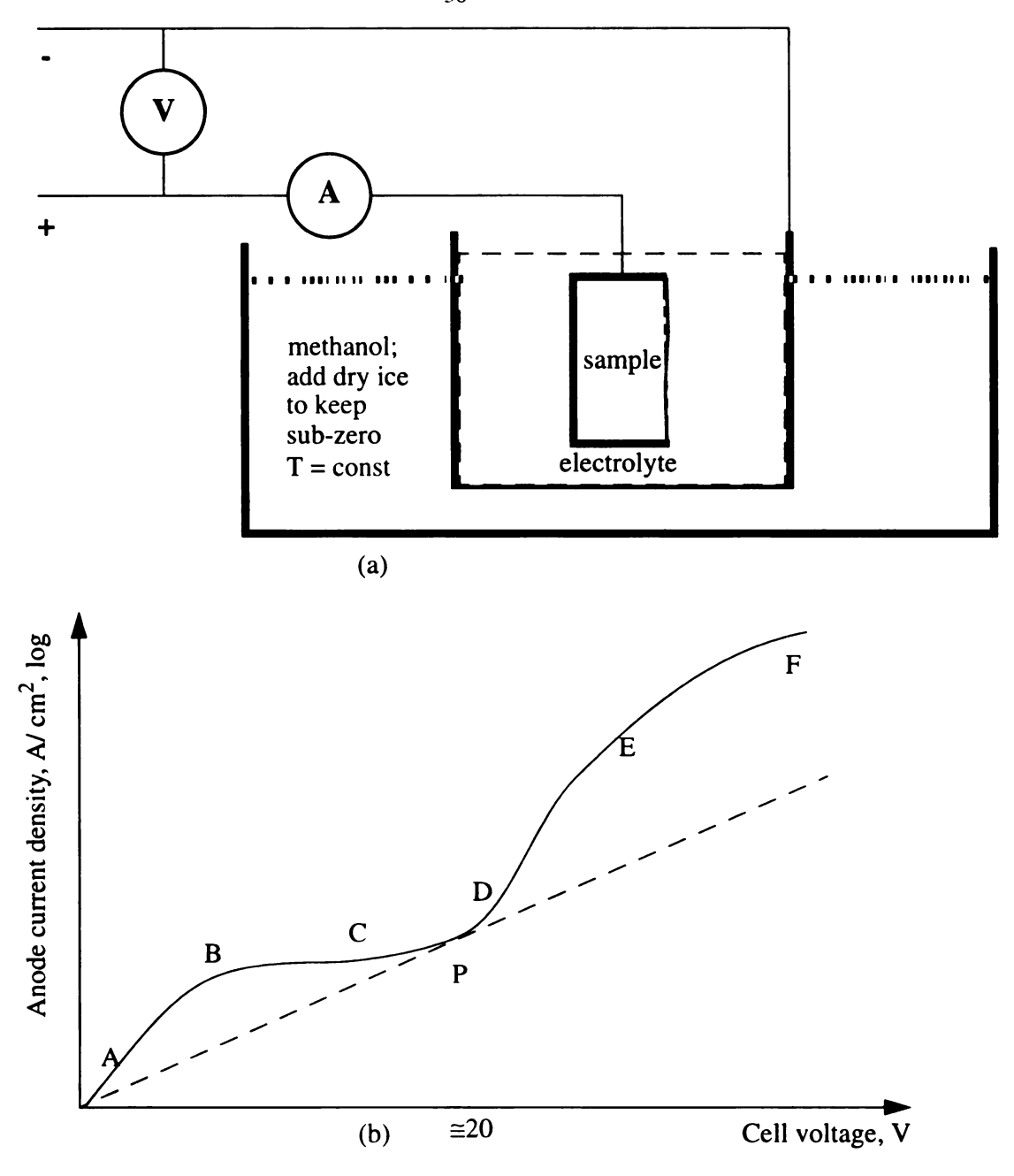


Figure 15. Electrolytic polishing technique

- (a) a simple electropolishing cell,
- (b) general form of the relation between cell voltage and anode current density. Regions relate to the following anodic processes: A-B etching; B-C instability; C-D polishing; D-E slow gas evolution with pitting; E-F polishing with rapid gas evolution. P indicates optimum polishing conditions.

- etching (<< 20 V) preferential attacking of structural features in the specimen
- pitting (>> 20 V) gas evolution from the specimen that disrupts the polishing layers.

For the electropolishing, the following electrolyte was used: 138 ml distilled water, 700 ml ethanol, 100 ml 2-butoxy-ethanol (also known as butyl cellosolve and ethanol glycol monobutyl ether), and 62 ml of a 70% solution of perchloric acid (HClO<sub>4</sub>) [22]. It should be noted that perchloric acid-ethanol mixtures are explosion hazardous, and that laboratory safety precautions should be strictly applied.

A sub-zero electrolyte temperature (about -10 °C) was used for electropolishing to facilitate control and safety. A liquid methanol and dry ice (solid CO<sub>2</sub>) bath was used. It was found that a higher temperature increased the amount removed in a time interval, but lower temperatures ensure uniformity in the polishing process.

The specimens were thoroughly washed in several dishes of acetone to remove the lacquer layer that covered all but the polishable sample surface. Then the samples were carefully rinsed in ethanol. All samples were polished for fifty minutes. By covering a part of the sample edge with acid resistant lacquer, and subsequently polishing the sample for 50 min, a distinctive step due to electropolishing was obtained and the actual average polishing rate of the electropolish under given conditions was evaluated. SEM examination of the samples found a step height was approximately 350  $\mu$ m after 50 min of polishing. This indicates an electropolishing rate of approximately 7  $\mu$ m/ min for the electrolyte and temperature used.

#### 2.3. EBSP collection

The EBSPs were collected using a Hitachi S-2500 scanning electron microscope.

Two different EBSP acquisition configurations were used and are described in detail later.

The EBSPs were formed using a sample tilt of 70° and a stationary electron probe.

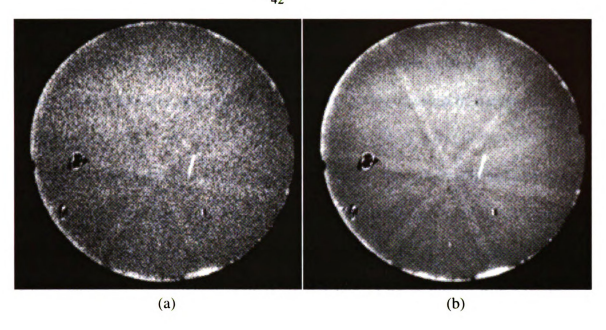
Optimum images were collected using a condenser setting of 1, working distance of 25 mm, and accelerating voltage of 25 kV.

#### RESULTS AND DISCUSSION

### 3.1. EBSP signal acquisition system development with SEMPER 6.4 software

This study is concerned with establishing the best approaches to evaluate micron-scale plastic strain deformation of bulk aluminum materials. The initial objective of this research program was to enhance the quality of EBSPs obtained on the Hitachi S-2500 SEM ( $E_{max} = 30 \text{ kV}$ ) and to develop the procedures for obtaining quantitative measurements of plastic strain from these enhanced patterns.

The setup initially used was the LINK ANALYTICAL EBSP analysis system, which consisted of an AN10,000 processor, EBSP analysis software and a low light level TV camera MERLIN LTC 1162F40 that monitored patterns by viewing scintillations of a phosphor screen in the vacuum chamber of the Hitachi S-2500 SEM. A TV camera control unit Type CCU 1552 performed contrast expansion of the image, flattened out the variation in intensity across the pattern, and generated a signal to pass on to the AN10,000 TV monitor. Even though the system works in real time and lets researchers obtain qualitative data from some materials (FeAl, Si, GaAs), it was found that the EBSPs on the TV monitor are too noisy for further quantitative analyses, as illustrated in Figure 16. With this system, EBSPs from light metals like Al, can not be consistently obtained; the EBSPs are too noisy to clearly see the bands. Consequently, signal image enhancement and processing were necessary to proceed with quantitative work. After evaluating the options available, it was decided to use the Semper 6.4 image processing software run on the 486/50 MHz PC platform in conjunction with the Synergy image processing subsystem. The Synergy subsystem is a single PC/ AT compatible board which can



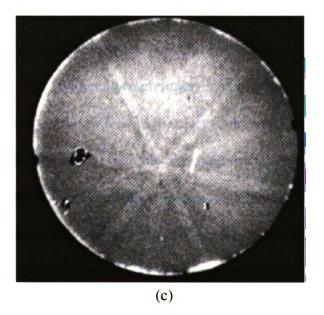


Figure 16. Semper "live" command captured EBSPs of electropolished Al:

- (a) captured single frame,
- (b) image enhanced by recursive filtering over 30 sec,
- (c) same as (b), after background ramp removal and histogram equalization.

display information at a resolution of up to 768 x 512 pixels. The displayable video pixel resolution is 8bits/ pixel. Synergy allows for full TV rate frame grabbing. Synergy can also carry the signals for slow scan operation that is commonly used in scanning electron microscopy.

The Semper software [44] has been developed to suit universal image processing applications and includes a high level image processing language. One can use Semper to perform image processing operations by typing commands in a special language: the Semper language. The language permits manipulation of whole images with a single command. The language is "high level"; the commands are given at the level the user thinks about the problem, not at the level of operations on individual pixels in the image. The software is user friendly. Some image processing systems use a collection of program subroutines written in a conventional programming language, e.g., Fortran. To use these subroutines, it is necessary to know how to translate each image processing problem into subroutine calls and to know how to compile, link, and run the resulting program on a particular machine. The Semper computer language is interpreted; the commands given to the computer can be decoded one by one and immediately executed. This is the same as the "BASIC" language can be interpreted. In contrast, "Fortran" or "C" programs must be passed as a whole through another program (a compiler) before they can be run. Thus, the Semper language properties allow one to try out ideas quickly. When the solution to a problem is found, it is possible to build Semper commands into a program (for example a Fortran code) which can be subsequently used any time.

As an alternative to typing commands, the Semper program can be controlled by means of a visual user interface, such as menus. Semper can be described as a portable,

complete operating environment. When Semper is started, the user enters a new operating environment. All the commands typed or entered through the visual user interface are interpreted by Semper. For practical purposes, one can assume that Semper replaces the computer's operating system (DOS or Windows for our 486 PC) with its own, which is dedicated to image processing. Any platform (UNIX, Macintosh, MSDOS) running Semper will respond in the same way to the same commands. Also, it should be noted that a temporary shell exit to DOS is possible.

Using the Semper/ Synoptics system in conjunction with the LINK installation it was possible to perform live image capture. After getting an EBSP image on the LINK AN10,000 TV monitor, the TV signal can be captured off the TV camera control unit output. Thus, after activating the framestore and camera connection, live image capturing can be performed with the captured image being displayed on an auxiliary monitor, as shown in Figure 17.

To install the Semper software, it was necessary to configure and edit the DOS, system, and framestore configuration files (config.sys, autoexec.bat, synergy1.cfg), and to fine-tune the hardware and software. One particular difficulty was in making the system self-compatible with the PAL (a European TV standard) and NTSC (the American TV standard) systems used by different devices in the setup.

One of the problems was the image "rolling" or flickering in the vertical direction on the display monitor whenever the framestore and videocamera connection was activated. It was determined that the Semper documentation was simply wrong.

Instead of the manual's indicated synergy.cfg configuration file, the semper.run file must be changed in order to alter the video standard, and consequently, avoid "flickering".

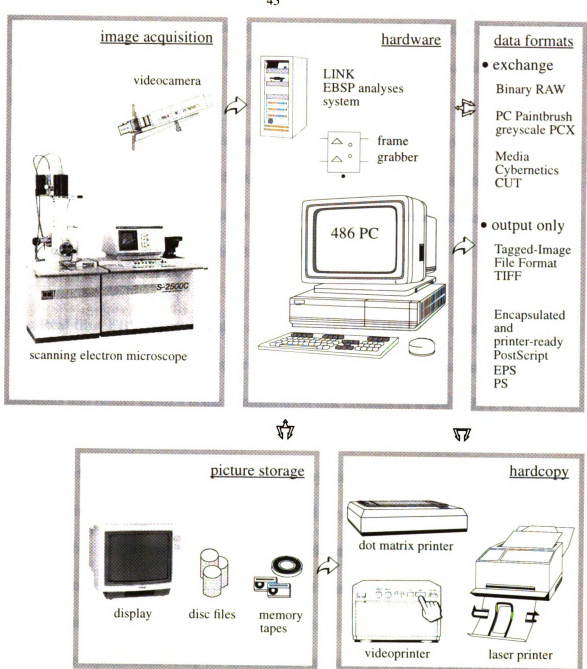


Figure 17. Real time EBSP capturing configuration.

The correct semper.run file is presented in the Appendix A. Similarly, to avoid flickering, when running tutorial, the option <ccir> should be added to the line <assign display> in in the tutorial.run file.

Having features of an operation-system, Semper primarily is software for universal image processing operations. A short summary of the most important Semper maintenance and interface commands gathered from the numerous manuals and trial-and-error are presented in the Appendix B.

# 3.2. Real time EBSP capture using a videocamera and the LINK system

One of the two experimental configurations used to capture backscattered electrons and render EBSPs is the configuration that consists of a low light level TV camera MERLIN LTC 1162F40 that views scintillations of a phosphor screen and is attached to the LINK camera control unit. This system is rather noisy, but has the primary advantage in that it can capture the EBSPs in real time. Using this system, it is possible to instantly observe changes in the patterns as the electron probe is moved from region to region. If necessary, the images may be grabbed into the Semper signal processing software run on the Semper PC.

The experimental setup for this method is shown in Figures 1 and 17. The electrons are scattered by atomic planes aligned at the Bragg angles, resulting in cones of excess electrons leaving the sample. These cones intercept a phosphor viewing screen mounted inside the microscope to form a series of lines. If structure factor considerations permit, one pair of lines is formed for each set of crystal planes. The pairs of lines form bands that intersect at brighter areas which correspond to the crystal zone axes.

The phosphor is monitored through a lead glass window by the TV camera with a gain of 500,000 [45]. The screen is placed approximately 50 mm from the specimen which is tilted 20 degrees from glancing incidence with the electron beam.

The camera control unit is provided to perform contrast expansion of the image, prior it to being input to a monitor. The system is controlled by the LINK AN10,000 computer, which differs from IBM, Macintosh or UNIX machines. The computer controls the LINK system, EBSP acquisition, and can perform EBSP pattern simulation. In the present study most of the work was carried out on aluminum. An EBSP map of Al, simulated using the LINK system, is shown in Figure 18. A rectangle is drawn around the area that is used for quantification. Normally, the LINK system monitors the TV camera in real time. The EBSP data come as varying electrical signals from the detector.

Therefore, it is easy to modify this signal with an amplifier. For example, the simplest EBSP on-line processing involves the adjustment of image brightness and contrast using a linear amplifier. However, the advantages of these convenient simulations are outweighed by a major LINK-videocamera system disadvantage - a low signal-to-noise ratio.

In normal operation, the signal-to-noise ratio can be increased by averaging. As the beam scans the specimen, the corresponding pixels are momentarily illuminated. This transient reading is transferred into a computer memory. Thus, after a complete scan, a digitally recorded (digitized) image is obtained. The computer will usually require as many data storage locations (bytes of memory), as pixels. Each pixel can store the intensity as a number between 0 and 255 for an 8 bit computer. The framestore is designed to transfer data rapidly to a monitor screen, so that the stored pixel data is represented as a point of the appropriate intensity on the screen. Framestores can be used

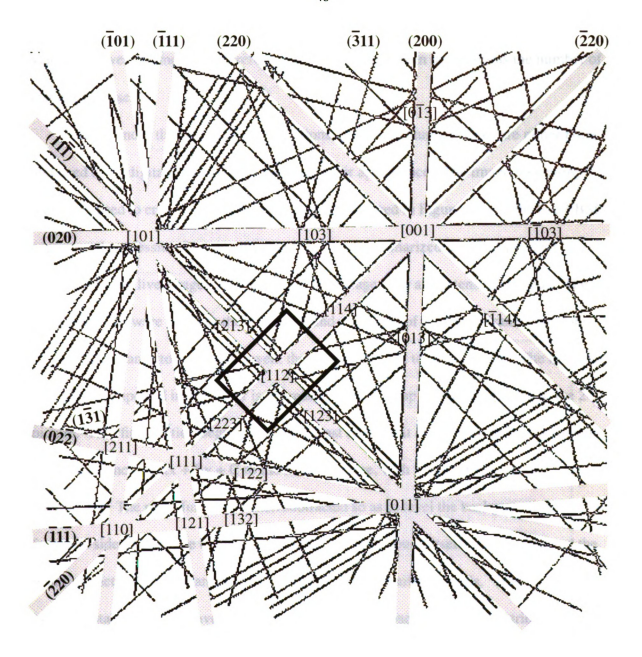


Figure 18. LINK system simulated aluminum EBSP map.

Accelerating voltage = 20 kV, angular width = 90 deg, central zone = <112>.

A rectangle is drawn around the area that is used for quantification.

for frame averaging. In this mode, the data in the frame store is updated to an average value after every frame, and, therefore, the noise on the screen decreases as the number of frames increases.

Even under the best imaging conditions, the live captured images are rather noisy and need to be digitally processed to improve their appearance. The image processing algorithm used to enhance live-captured images is showed in Figure 19, and the live EBSP capture and processing Semper commands used are summarized in the Appendix C.

When capturing live images, it is necessary to average over a few tens of seconds. The Semper 6.4 software controls the averaging and digitizing of incoming framestore data.

After framestore data are saved, they typically have to be enhanced. The first step on a picture imported into Semper is to create a linear ('ramp') function that fits to the 2-D picture. The 'fit' function begins by using a least squares fit criterion to fit the coefficients of a linear function Ax + By + C to the source picture, with x and y being picture coordinates. The ramp function is then subtracted so as to level the background variations from one side of a picture to another. Finally, the background itself is subtracted and the resulting picture's histogram is stretched to fill all 256 available levels. Both experimental and digital (averaged over 40 x 40 pixels) backgrounds were tried.

Somewhat better results were obtained by subtracting the digitally averaged background. The application of this image processing routine on live captured EBSPs is illustrated in Figure 16. The resulting EBSPs still are rather noisy. However, using this approach, EBSPs from different samples can be compared qualitatively. A number of different signal enhancement algorithms were tested on the camera and images captured with the LINK system configuration. The algorithm presented in Figure 19 gives the best results.

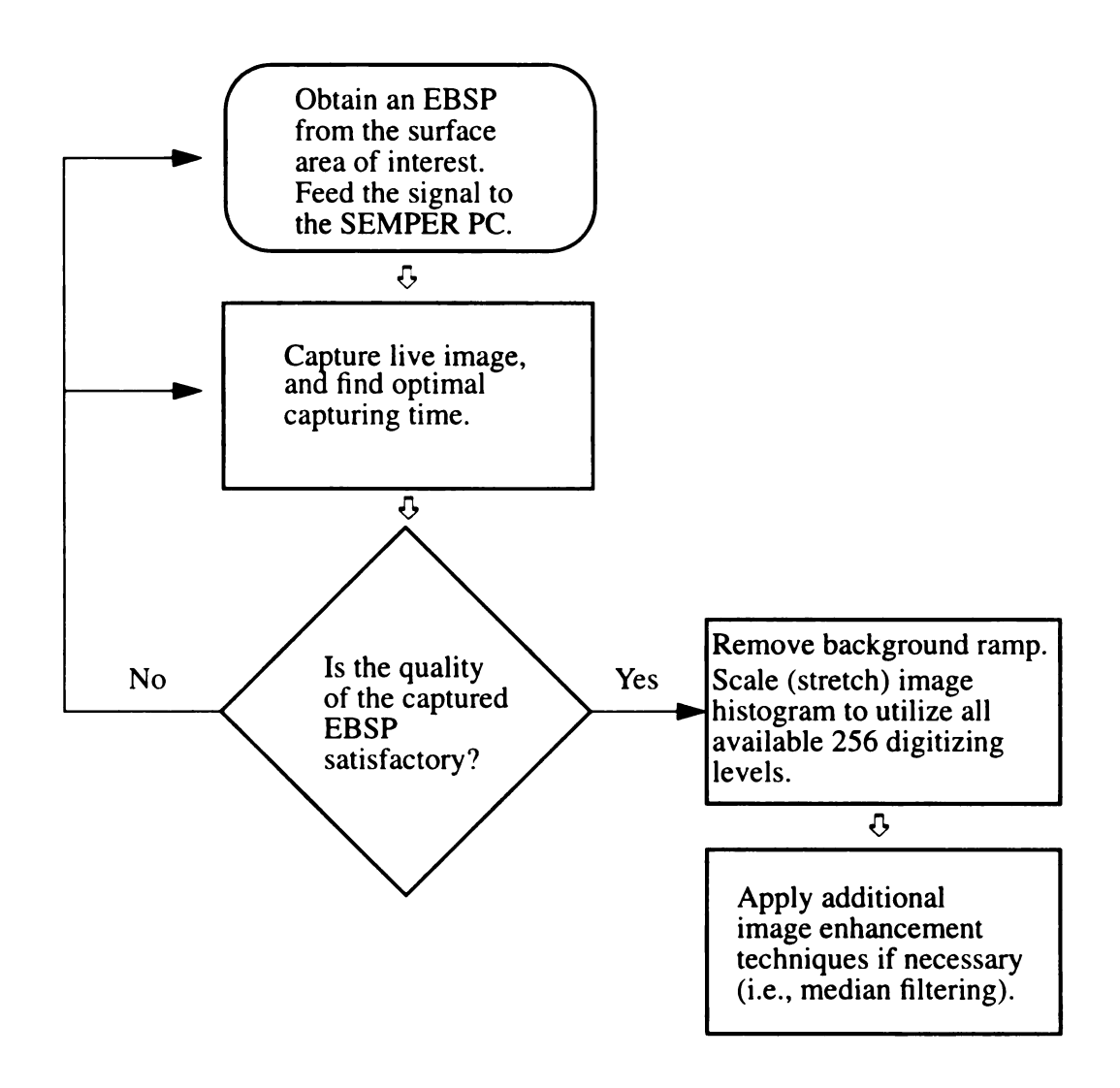


Figure 19. Digitizing and enhancing algorithm used in LINK controlled TV camera live capture of EBSP images. Semper commands are presented in Appendix C.

It is concluded that the capabilities of the hardware have been optimized, and further improvements require less noisy hardware in order to do quantitative EBSP analysis with a TV camera.

Even though the system is not suitable for quantitative measurements of the light aluminum, it has the great advantage of obtaining real time EBSPs that can be compared qualitatively (as opposed to quantitatively). Also, the EBSP pattern LINK simulation software is very user friendly and convenient to use. Moreover, there are situations (texture analyses) where the direct correlation between the area of the sample from which the pattern originates has advantages over substantially more precise and quantitative, yet considerable slower, photocamera method considered in the section 3.4.

### 3.3. Correlation between the surface quality and the EBSPs

When the quality of EBSPs from aluminum needed to be improved further, apart from increasing the quality of the pattern rendering media, several sample preparation techniques were also pursued. The aim of this work was to correlate the surface quality with the EBSPs visual appearance.

For processes that depend on the ordered nature of the lattice, i.e., heavy ion channeling and proton scattering, the surface preparation requirements are even more stringent than those for the standard metallographic examination of surfaces and EBSP acquisition. Thus, there are developed sample preparation methods which allow for even further improvement in sample preparation. One particularly good review that touches upon a description of the many techniques available for the preparation of undamaged single crystal surfaces is "Target Preparation" by Whitton [43]. The review is on target

preparation in vacuum apparatus and is concerned with the channeling processes.

Cutting the annealed and deformed bulk specimens with a chosen cutting technique deforms the cut surface introducing an imperfect surface layer. For the purposes of this project, the depth of the surface layer disturbed by this process is important. Many experiments have been performed to determine the depth of damage [22, 23, 42]. The depth of damage is defined as the depth below which the dislocation density had not been appreciably increased by cutting. Recalling that the EBSP technique draws information from less than a 1µm thick surface layer of the soft aluminum, some typical numbers on the thickness of the damaged layer should be considered. A conventional hacksaw, even with fine teeth, would do significant damage and may easily affect the structure as deep as 1 mm in a soft metal.

Three less damaging cutting techniques are electrodischarge machining, which uses a low energy spark, diamond wafering cutting, and the least damaging, but most difficult technique, acid saw cutting, in which a moving string carries acid (or some other appropriate solvent) through the cut [46, 47, 48]. All three methods were tested, and each one of them has advantages and disadvantages.

The acid saw cutting method is very gentle since the action is essentially chemical rather than abrasive, but as a result, is rather difficult to control. For strain-free cutting the technique utilizes localized chemical attack induced by the continuous introduction of fresh reagent to a local area. Acids or solvents are used which readily attack the crystal to be cut, but which do not attack the 0.005 inch diameter stainless steel wire used to draw the acid. In the present study, 20% sodium hydroxide solution was used for cutting aluminum. The technique allows cutting without introducing dislocations, but the cut

surface undulates on the mm scale. It is, however, smooth enough for EBSPs, which require smoothness on the micron-scale. Examination of section planes by the double-crystal spectrometer technique has shown that the maximum penetration depth of the dislocations produced using acid saw is about 30 µm for metal and ionic single crystals [49]. The acid saw in the Physics Department works very slowly and needs constant attention as the motor has a slight eccentricity and the solvent carrying wire's movement causes the wire to dislodge from the pulleys from time to time. A new motor could fix this problem, and, provided the machine's performance was stable enough, the cutting speed is not prohibitively slow.

Electric discharge machining (spark cutting) uses a mechanism of erosion through local melting of the specimen and ejection of the molten drop from the surface. This results in a cratered surface, the roughness of which depends on spark energy. The spark machine also employs a moving wire. In a spark machine, the specimen and cutting wire are immersed in dielectric oil and a high voltage spark is established between the moving wire and the workpiece. A servo mechanism is used to maintain the spark gap between tool and specimen at an appropriate value and there is never any physical contact between the two. Deformation of the specimen is limited to the region close to the spark-melted area.

The depth of damage using a low energy spark, corresponding to the finest range on a Metals Research Ltd. Servomet SMD, has been found to be less than 2  $\mu$ m in silicon iron, less than 10  $\mu$ m in tungsten, and 80 - 300  $\mu$ m in copper [50]. Therefore, it is essential when cutting soft metals to use the lowest energy spark available and to ensure that at least a few hundred micron layer is removed from each surface by subsequent

damage-free thinning techniques. Spark machining can only be applied to conductors and even though it tends to be slow, is considerably faster than acid saws.

During this study, a Materials Science Ltd. MK-II Spark Erosion Unit<sup>TM</sup> was used.

The spark cutting machine allows the cutting of samples with different spark energies.

For test purposes, an aluminum sample was cut with the lowest spark energy (setting 1) and somewhat higher energy (setting 3). Even though the surface was macroscopically much smoother in the former case, the EBSP patterns were better for a higher energy setting 3, as shown in Figure 20. This seemingly contradictory result can be explained by considering structural changes introduced by the EDM in the 1µm surface layer measured by EBSP. When the spark energy is higher, the molten layer is thicker. The molten layer cools down slower and recrystallizes forming a fairly uniform crystalline layer in turn which yields better quality EBSPs.

Following the spark cutting stage, the spark cut surface should be electropolished.

Spark cutting is a viable option for initial cutting of material, provided some improvement of the wire path setup are made.

A diamond wafering wheel is the last of the three less damaging sample cutting techniques. This method is the fastest of the three and also introduces the most damage. For hard materials, it is possible to restrict the damaged layer to a few tens of microns [23]. It was assumed that for softer materials, such as aluminum, the damaged layer thickness should not be more than a few hundred microns. A few hundred microns thick surface layer can be removed by polishing and electrochemical polishing. After considering all three methods, it was decided in favor of the diamond wafering wheel for initial sample cutting.

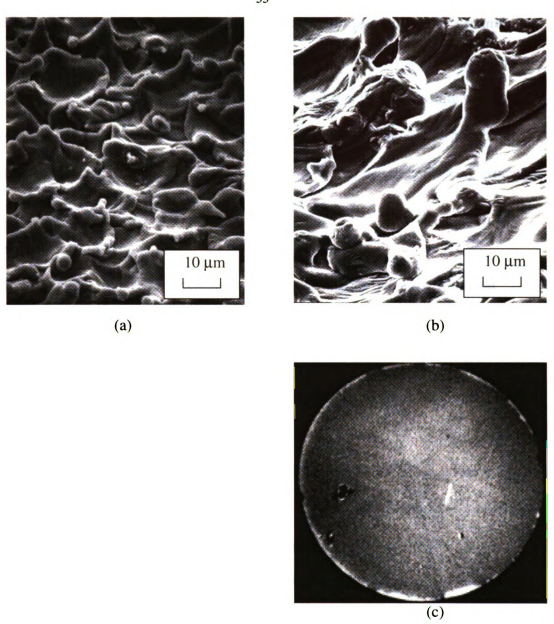


Figure 20. Electron discharge machine spark's energy influence on the Al samples EBSPs quality

- (a) SEM micrograph of the cut with the lowest available spark energy (setting 1),
- (b) SEM micrograph of the cut with higher spark energy (setting 3),
- (c) corresponding EBSP pattern obtained from surface (b) with the LINK system,
- (only background noise is present in EBSPs corresponding to (a)).

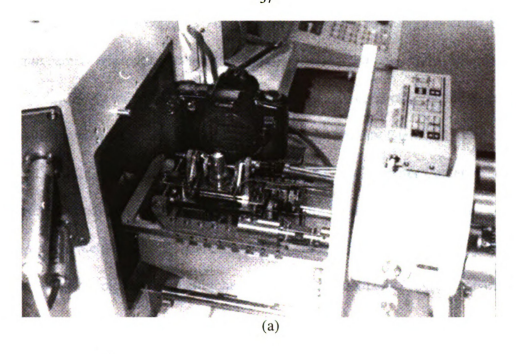
## 3.4. High quality patterns acquisition using a fine grain photofilm and a scanner

The key to improving the quality of acquired EBSPs quality was to determine where the signal gets most heavily degraded by noise of the image acquiring system (Figures 11(a) and 17). When the source of the additive noise term is determined, the signal/noise ratio can be improved. This thesis research revealed the following critical EBSP signal degradation sources:

- sample preparation quality,
- LINK system introduced limitations (white and the needle-like noise of digital systems, non-satisfactory analog-to-digital conversion).

The first problem can be overcome by finding the optimum sample preparation technique for the sample material. The second problem can be solved by circumventing the LINK system ADC.

In collaboration with Mr. A.W. Gibson and Professor M.A. Crimp, a solution to the second problem was developed. For the first time, a commercial photocamera body was put directly in an SEM chamber (Figure 21) to facilitate EBSP capture [40, 51]. In conjunction, Kodak<sup>TM</sup> fine grain positive release 35 mm film was chosen as the EBSP capturing media. Using this configuration, an approximate specimen-to-film distance in the actual setup was measured to be 70 mm. Using the geometry of the setup (Figure 21) and general EBSP forming principles (Figures 1 and 2), it was determined that on a standard 35 mm negative approximately 20 degrees vertical range and 30 degrees horizontal range can be captured (see also Figure 18). By using a Canon remote switch, the camera body can be activated, different exposure times applied, and the film rewound without disturbing the microscope vacuum. The resulting EBSP quality was outstanding



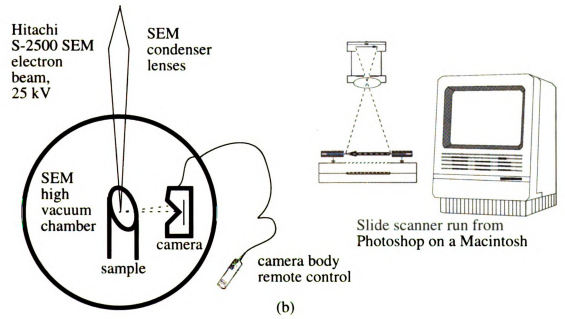


Figure 21. High quality EBSP's capturing configuration

- (a) photocamera and sample geometry in the SEM chamber,
- (b) overall system layout.

when compared to EBSPs captured using the TV camera based camera system. Hence, the 35 mm camera approach was used for quantitative work in this study. In order to process and quantify the EBSPs collected using the 35 mm camera body, the negatives were digitized using a LeafScan negative scanner at the Faculty Facility for Creative Computing (FFCC) Laboratory, Michigan State University Computer Center. The image levels were then adjusted in the same, uniform way for all images. The images were transferred into the Semper PC where the image background ramp was subtracted. The resulting image histograms were stretched to use all 256 available greyscale levels. The signal processing algorithm used in 35 mm negative digitization is shown in Figure 22.

The LeafScanner was controlled from Adobe Photoshop 2.5.1 run on a Macintosh computer. The negatives were scanned using a 8-bit greyscale digitizing and resolution of 400 dots-per-inch, which corresponds to approximately 65  $\mu$ m/pixel resolution on the negative (Figure 23(a)). The Semper system can render images with 768 x 512 pixels. A scan size of 4.88 x 3.25 cm was used for all of the images. The resulting file size was approximately 768 x 512 = 393 Kb.

In Photoshop 3.0 the EBSP images were rotated and cut as necessary, as shown in Figure 23(b). The image levels were auto adjusted. Finally, the files were ready to be transferred from Photoshop (run on a Macintosh) into Semper (run on a PC). In order to avoid loss of pixel-by-pixel stored data, the files were transferred in the raw binary format (byte stream). In the byte stream form, information is preserved at the pixel level and no compression is applied. Thus, it is necessary to input the image size when a raw binary file is opened. The computer accordingly cuts the byte stream and forms lines. When the data are transferred over the network, the file transfer protocol (ftp) is used and the raw

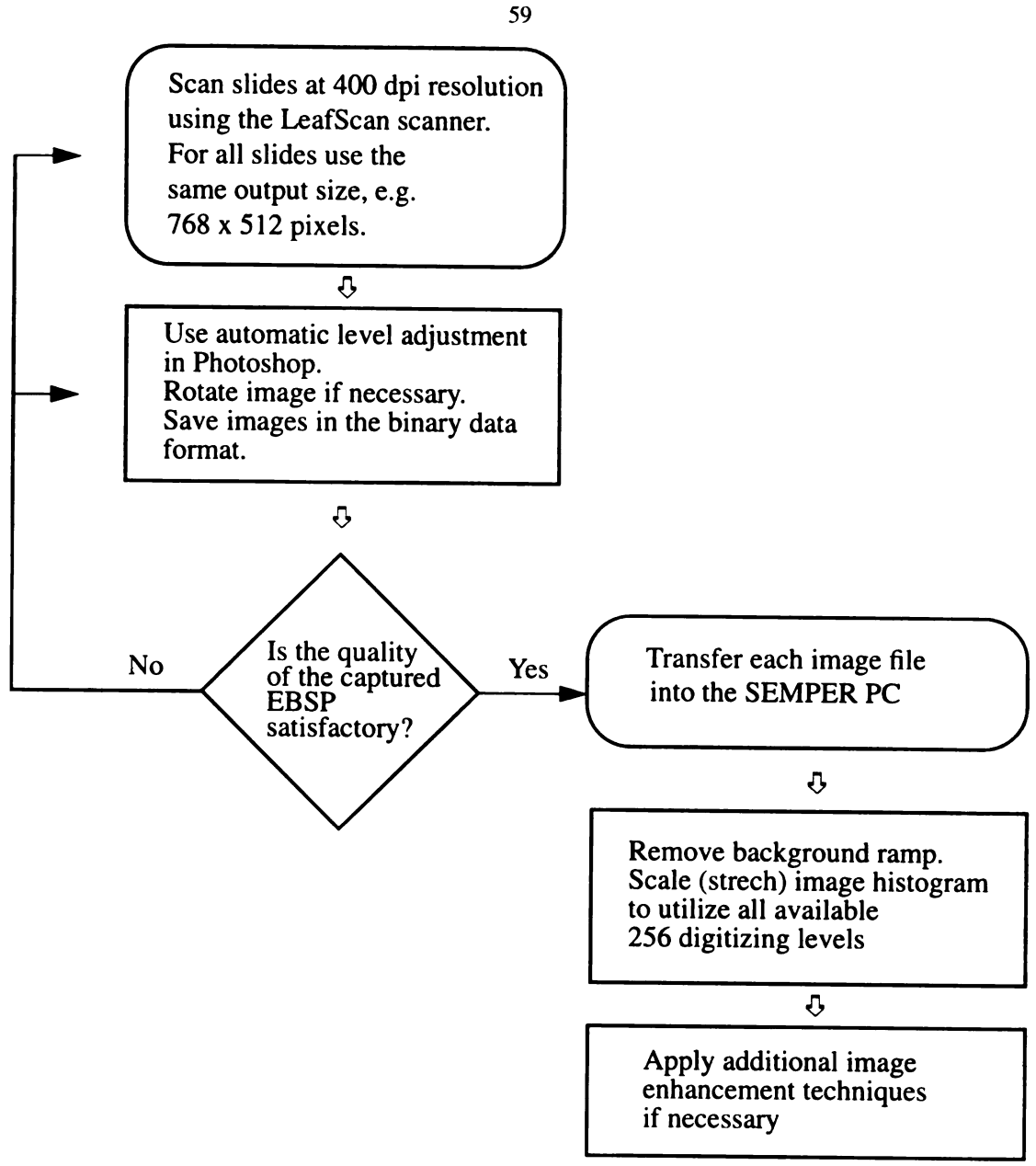


Figure 22. Signal processing algorithm used in slide digitizing.

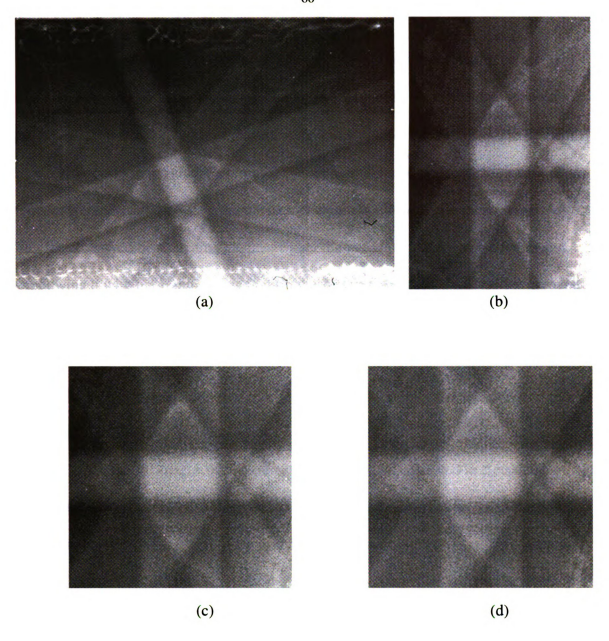


Figure 23. Representative Al EBSPs at different steps of digitizing

(a) an EBSP as-scanned,

(b) same as in (a) after rotation, cropping and automatic level adjustment,

(c) same as in (b) after extracting a 256 x 256 p square and resetting the outliers,

(d) same as in (c) after removing the ramp and image stretching. Image mean is set to zero.

data transfer option must be chosen.

When the files were in the Semper PC, the background ramp was removed by using the Semper fit command and the images were stretched to fill all 256 available greyscale levels (Figure 23(c)). First and second order EBSP band profiles can be clearly seen. After background gradient removal the intensity of very bright and very dark pixels (outside 3 standard deviations from the picture mean) was reset to the mean image value. This was followed by stretching the image over the available 256 greyscale levels and windowing it with the Hanning function (in the 2-D PSFM case). Then, the background ramp was removed again. Finally, the mean image intensity was set to zero (Figure 23(d)) and the EBSPs were ready for Fourier transform (FT) and PS parametrization.

#### 3.5. EBSPs diffusiness quantification

Only after the images from different samples can be enhanced in the same, standardized way, can EBSP quantification be initiated. One particular quantification application is the measurement of the distribution of plastic deformation. To compare EBSPs from different samples, a particular zone must be taken as a common feature. The EBSPs quantifying approach based on the Fourier transform (FT) [7, 8, 35] is followed in this thesis. An alternative approach exists [52] which argues that EBSPs, like electron channeling patterns, should be measured in the Hough space. The argument is that both EBSP and channeling patterns are not really periodic functions; therefore, FT methods seem to be less suitable. In this study, the bands around the <112> zone (Figures 18 and 24) were taken as the common feature and quantified. The contrast of the main band was assessed using the enhanced images by measuring the intensities along the (311) band as

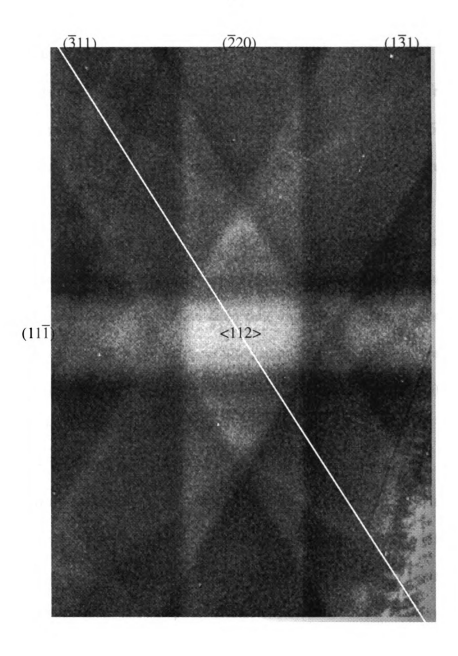


Figure 24. Indexing of aluminum (fcc) bands around the <112> zone. The white line depicts the line along which (the  $(\overline{3}11)$  band) the patterns were extracted in the 1-D SFPA case.

illustrated by the trace shown on Figure 24. The algorithm for obtaining SFPA values is shown in Figure 25.

Following this negative digitization procedure, the EBSPs obtained from the 99.999% purity polycrystalline Al samples deformed in compression at 0%, 5%, 14%, and 18% percents were digitized. The enhanced EBSP patterns are shown in Figure 26. Even at the largest deformation the EBSPs are seen. This is a very good result for a light element of a polycrystalline material. It is clear that the diffusivity of the patterns increases with the increase of strain. In other words, the patterns "diffuse out" with the increase of applied strain. EBSPs of the same zone are chosen for quantification. An interesting effect is that some bands appear tilted, even though in fact they are not. This is because some patterns are captured away from the negative center and the effect is determined by the gnomonic projection [53].

# 3.5.1. Spectral first peak area (SFPA)

The diffuseness of bands can be quantified by finding the area under the first peak of the power spectrum, or the spectral first peak area (SFPA), obtained from the projected average intensity profile of the band [34]. The sharp edges of the EBSP bands involve rapid changes in intensity. The sharpness of individual bands can be determined using the area under the first peak in the power spectrum obtained from the projected average intensity profile, as shown in Figure 27. The Hanning window function should be applied to the profile prior to transformation in order to emphasize the central Kikuchi band and to reduce leakage encountered in the use of discrete Fourier analyses. The SFPA coefficient value is determined as a fraction of the total spectral area and is, therefore independent of the pattern contrast and always less than one. The scatter between measurements

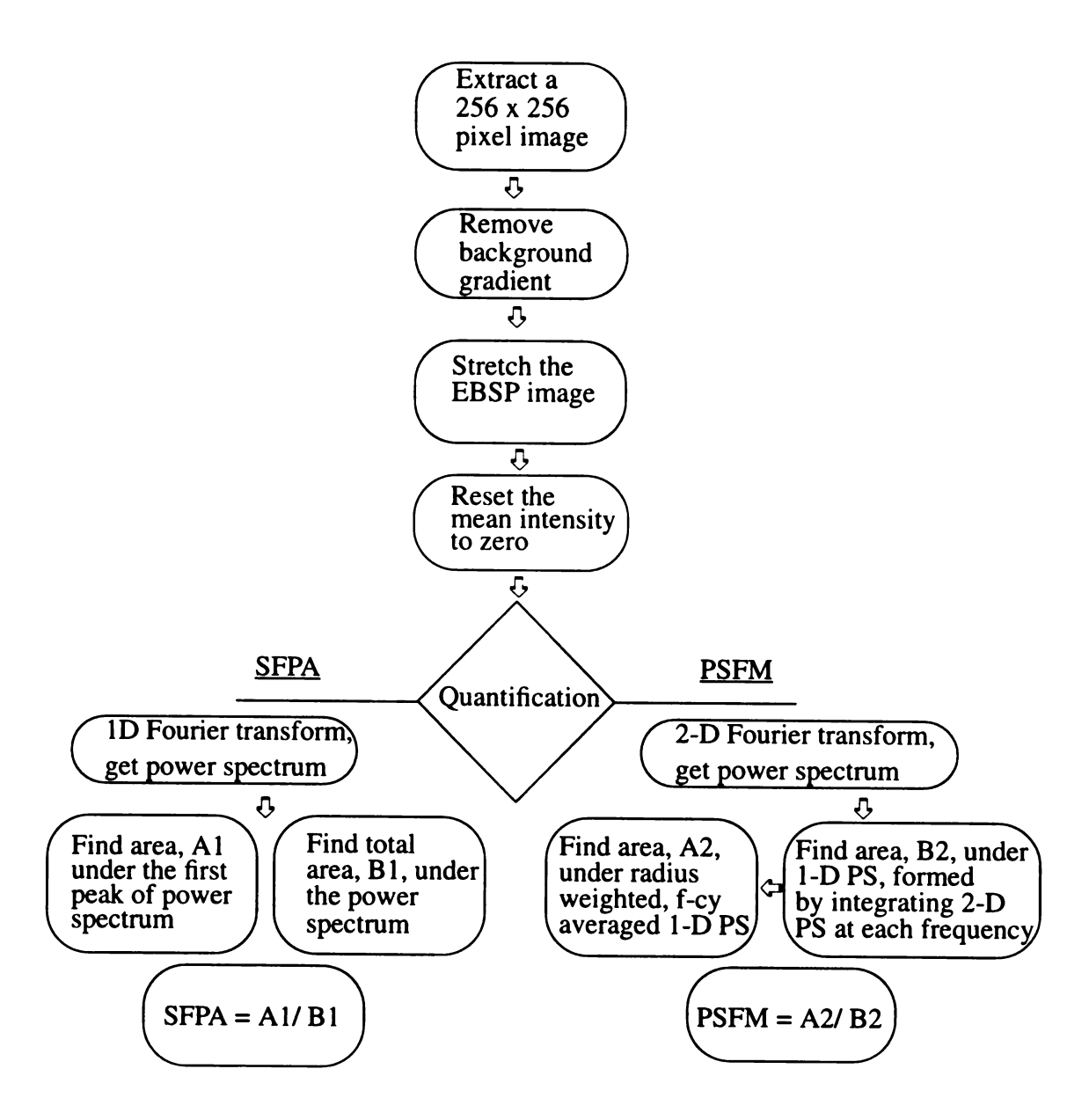


Figure 25. Electron back scattered pattern quantification algorithm.

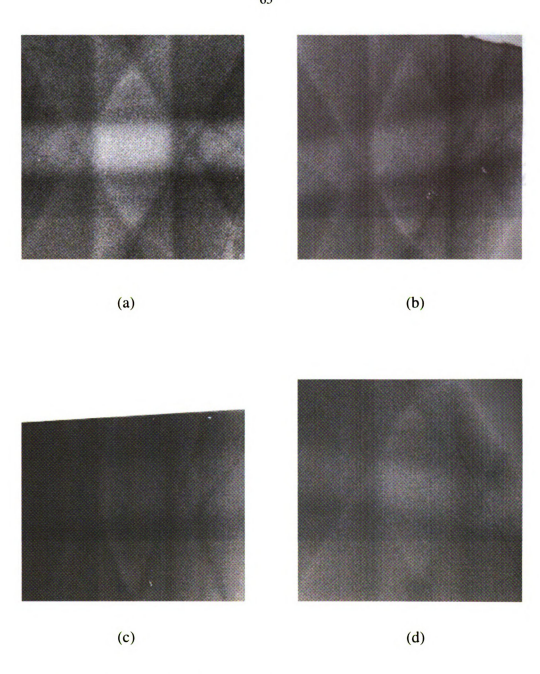


Figure 26. EBSP patterns from 99.999% purity Al deformed in compression to (a) 0%, (b) 5%, (c) 14%, and (d) 18%. All patterns were extracted around the <112> zone. The patterns tend to "diffuse out" with the increase of the amount of strain applied to the polycrystalline aluminum.

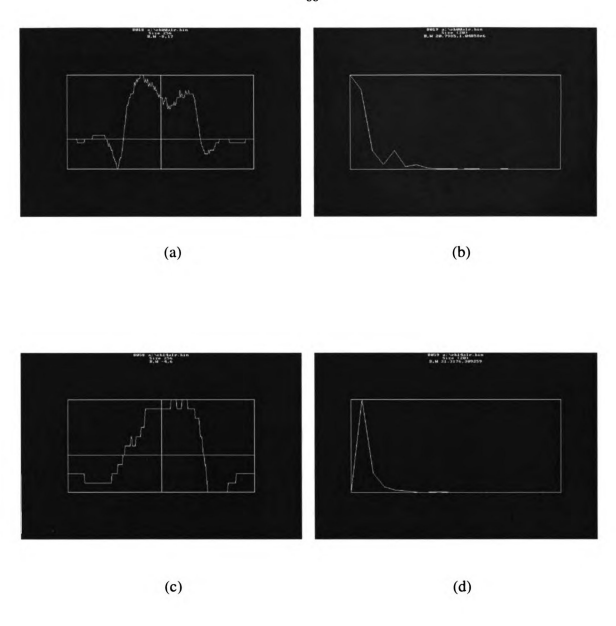


Figure 27. Average intensity profiles of  $(\overline{3}11)$  bands present in EBSPs obtained from (a) annealed and (c) 18% strained polycrystalline aluminum. The corresponding power spectra (b) and (d) illustrate the attenuation of higher frequencies from deformed material.

increases significantly with deformation, reflecting the difference in degree of deformation from grain to grain (see also Figure 26). The Semper commands used to quantify EBSPs with this technique are summarized in Appendix C. The SFPA method is highly sensitive to the position at which any one single profile is extracted. This dependency was reduced by averaging along a direction indicated via the cursor (over the entire length of the  $\overline{3}11$  band). The use of a 2-D Fourier analysis further reduces this dependence on position. The numerical values for the SFPA method for the same EBSPs are summarized in Figure 28. The EBSPs for larger strains are more diffuse and the SFPA method is able to quantify this diffuseness increase well (Figures 23 and 28). The SFPA should increase with increasing strain and this is in fact observed. The data points are fitted with the least squares method ( $R^2 = 0.9547$ ).

## 3.5.2. Power spectra first moment (PSFM)

The discrete Fourier analysis reveals that the high frequency components were decreased (attenuated) by plastic strain. Thus, the first moment of the 2-D power spectrum, or power spectrum first moment (PSFM), can be used to quantify the pattern sharpness and to generate a single value quantifying the quality of EBSP's band profiles [7, 8, 34, 39].

For all four images, the power spectrum was calculated. An example of the display of 2-D power spectrum is shown in Figure 29, where the frequency increases radially from the center and the pixel brightness depicts the magnitude of the Fourier component. The mean intensity level in the image controls the height of the zero frequency peak in the power spectrum; it has already been set to zero for each image. The stretching of the image over different max-min ranges does not affect the shape of the

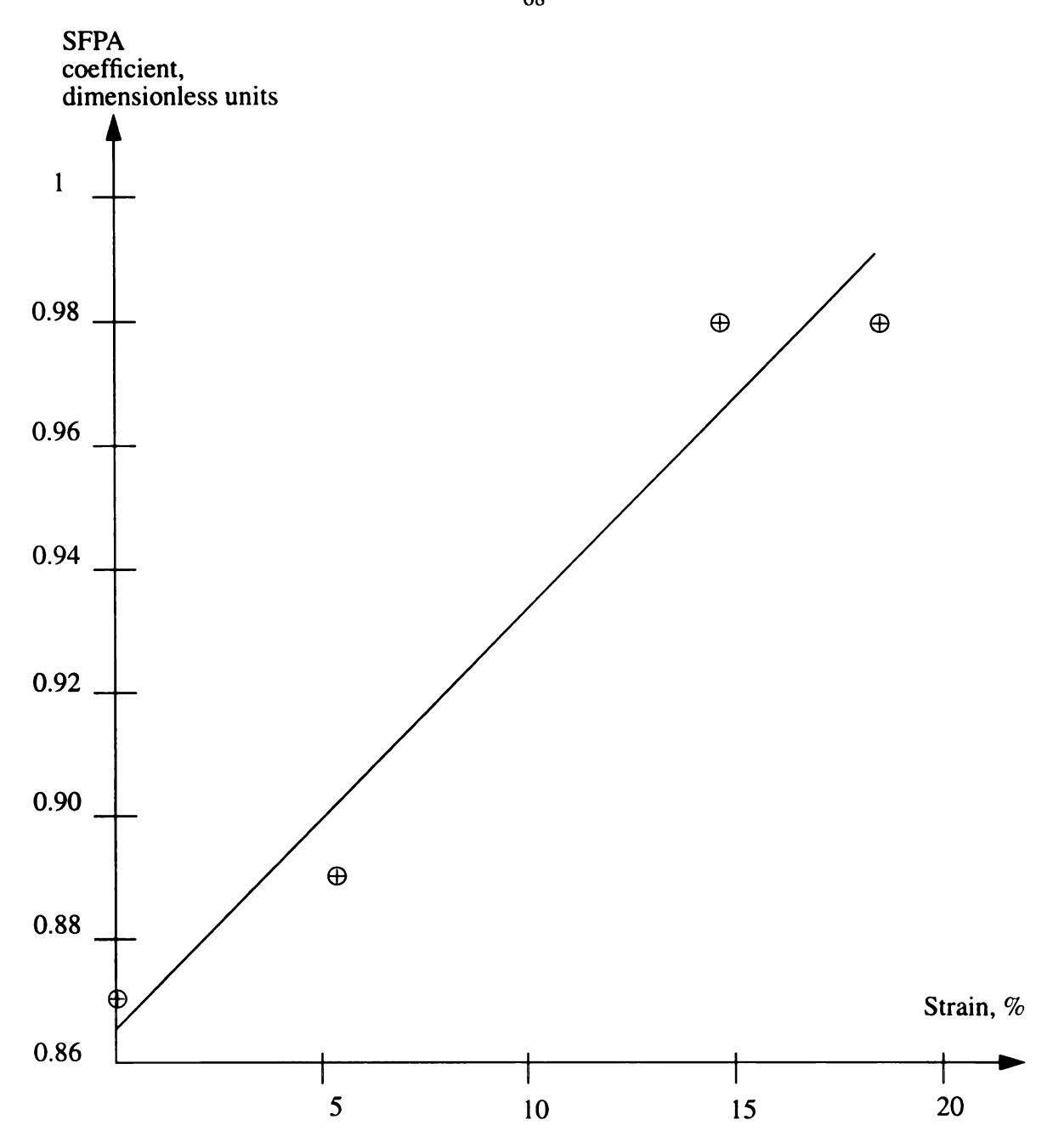


Figure 28. The correlation of sample strain with the measured values calculated following the SFPA method. The data points are fitted with the least squares method. The linear data fitting line parameters are y = 0.0068x + 0.8652;  $R^2 = 0.9547$ .

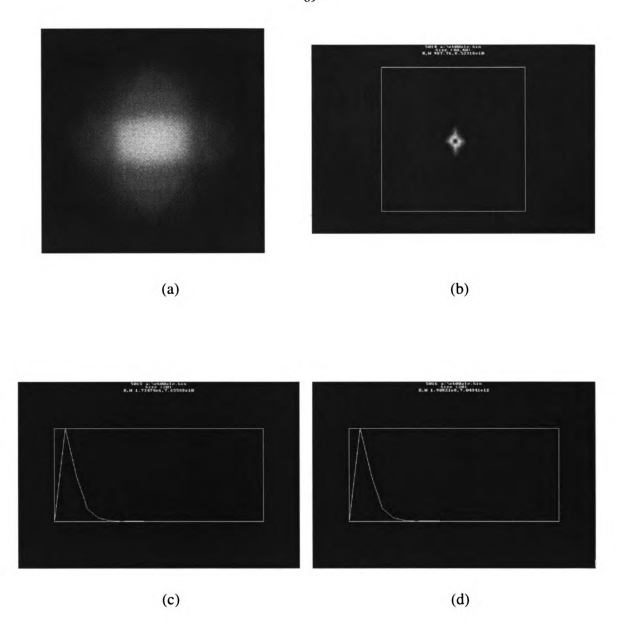


Figure 29. Representative steps of quantification using the PSFM method.

- (a) selected EBSP 256 x 256 pixel area masked with Hanning window function,
- (b) 2-D Fourier transform of the area in (a),
- (c) 1-D averaged at each radius 2-D PS in (b),
- (d) weighted PS formed from (c) by multiplying each coefficient by its radius.
- (A2 = area under the PS in (d)).

power spectrum, though it will alter the actual values of the coefficients. The PSFM value should be unaffected by such grey level stretches due to the first moment being divided by the volume under the 2-D PS. This, in fact, is the main reason for this term [34, 39]. Therefore, one should take care that the mean intensity level of the processed EBSPs be the same for all images, whereas the max-min range values are not critical.

Further integration of the 2-D spectrum around circular paths at each radii allows average coefficients to be determined at each frequency, which amounts to finding the average value at each radius in the power spectrum. Then the area B2, under the 1-D power spectrum, formed by integrating 2-D PS at each frequency, was found. The area was found by summing individual pixel values with a 'for' cycle. The 1-D PS is stored in Semper as a 256 x 1 matrix. Next, each coefficient in the average power spectrum was multiplied by its angular frequency (radius in Semper). This was done in order to form a "weighted power spectrum". Similarly, the area A2 under the weighted power spectrum was found. Finally, division of the first moment by the area under the spectrum was used as a means of removing any dependence on pattern contrast. Quantitatively, the coefficient of PSFM = A2/B2. The list of actual Semper commands used for the PSFM method are given in Appendix D.

The numerical values for the PSFM method for the same EBSPs are summarized in Figure 30. While SFPA should increase with increasing strain, the SFPA should decrease [7,8]. This is not clearly observed on Figure 30. The data points are fitted with the least squares method ( $R^2 = 0.0458$ ). Thus, in the study, the results of the PSFM method do not reflect the plastic strain as well as the SFPA method; the PSFM method has not been able to satisfactory quantify the diffuseness (Figure 30). This may be due to the

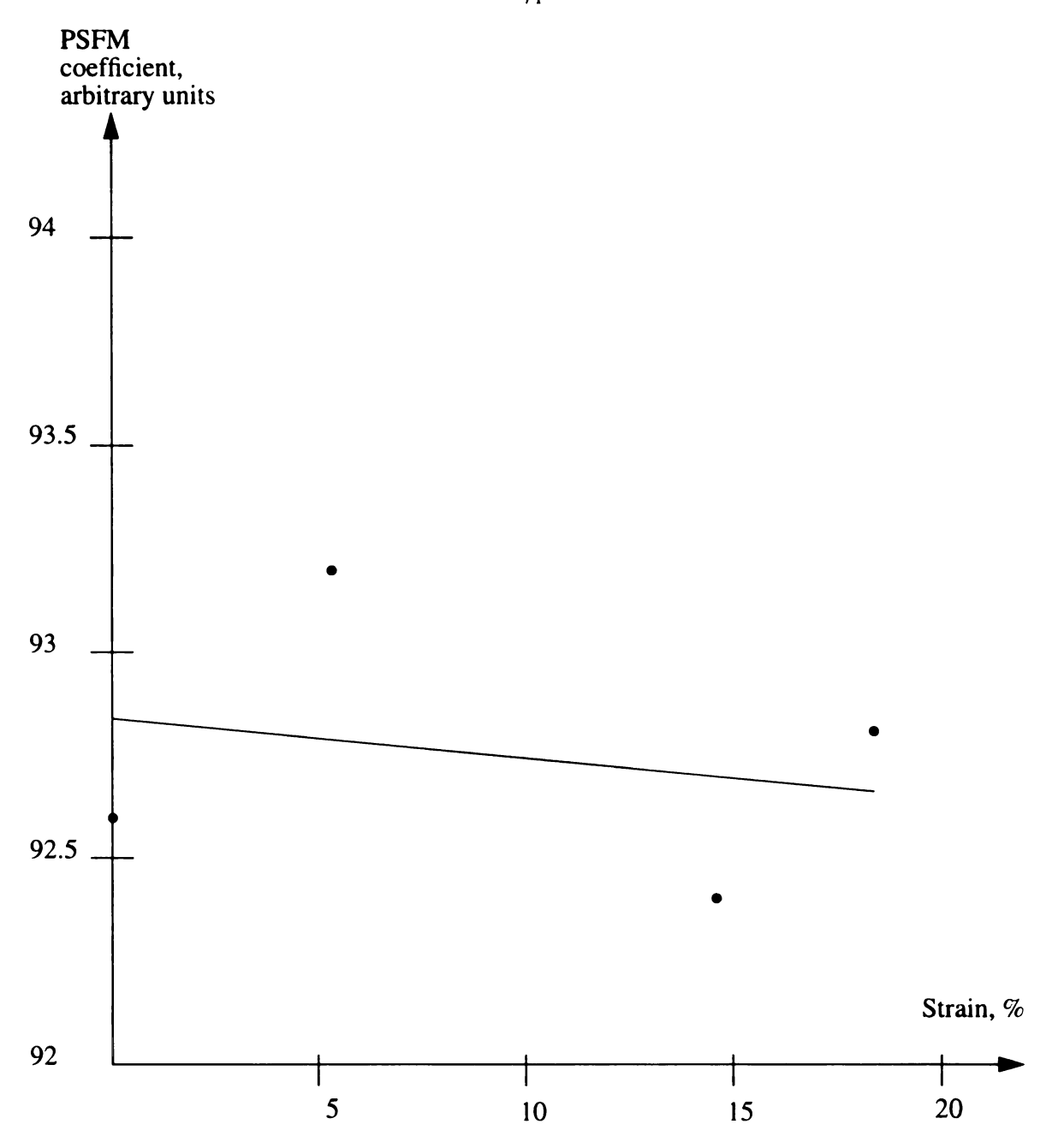


Figure 30. The correlation of sample strain with the measured values calculated following the PSFM method. The data points are fitted with the least squares method. The linear data fitting line parameters are y = -0.0087x + 92.833;  $R^2 = 0.0458$ .

fact that the applied Hanning function can not completely eliminate the effects of film imperfections (scratches and dust) and film edges. Each sharp discontinuity (like a scratch or an edge) will be accounted for in the overall picture Fourier spectrum. Also, physically similar patterns are represented mathematically in a different form. For example, because of the collection geometry, the angle between (11 $\overline{1}$ ) and ( $\overline{2}$ 20) bands is not always 90°, as they should be (Figures 24 and 26). Thus, inconsistencies avoided in the 1-D method, may be introduced in the 2-D FT used in the SFPA method. The more these discontinuities are present, the less reliable are the generated PSFM coefficients. These artifacts can be accounted for only with statistical methods.

#### 3.5.3. Evaluation of EBSPs diffusiness quantification methods

The EBSP quantification algorithms are summarized in Figure 25. Both approaches utilize the property of EBSPs to become more diffuse with increasing strain. The pattern diffuseness can, in turn, be compared in Fourier space utilizing the attenuation of the higher frequency Fourier spectrum components. This attenuation (weakening) of higher frequency components can be quantified mathematically by parameters that determine the engrossment of the first peak with regards to the all of the Fourier spectrum. In terms of the SFPA and PSFM parameters, this means an increase of the SFPA value and a decrease of the PSFM value, with increasing strain.

No statistical analyses of the results was carried out because of experimental difficulties involved in obtaining a statistically sufficient number of 20 x 30 degree film rectangles with the <112> zone well-centered. This is because while the 35mm camera body provides the quality images necessary for EBSP quantification, the lack of real time imaging with this method makes capturing a zone of choice a chance event. In the present

study a very large number (100-150) of EBSPs were collected from each of the strained samples. It should be noted that qualitatively, the trends of increasing diffuseness with strain was generally observed for these patterns. However, only a very limited number of images revealed the common <112> zone well-centered. Attempts to use the live TV system to orient samples prior to 35mm film capture proved less than satisfactory due to the different positions of the two systems in the SEM chamber. Future work should include developing a workable solution to this problem.

Despite these limitations, it should be pointed out that it may be possible to carry out many investigations with the present configuration. For example, it should be possible to examine the change in plastic strain as a function of distance from a reinforcement in a composite material, provided all of the EBSPs are collected from the same grain. That is, changes in the EBSP across a grain can be examined.

Thus, it can be said that the results are semi-quantitative and biased, for there is only one EBSP for each strain level. The individual EBSPs were obtained from randomly chosen grains, which may or may not have had plastic strain levels representative of the average plastic strain of the polycrystalline Al. With increasing nominal plastic strain, this variation in density and, arrangements of the dislocations (and associated strain), found in the different grains of the deformed sample should increase [34]. Thus, it is reasonable to expect the experimental scatter to increase with increasing nominal applied plastic strain and statistical analysis is necessary.

Summarizing, it can be said that the mathematical apparatus for both methods is developed, yet at present, the SFPA method gives better results. This means that even with the present experimental setup, micron scale plastic strain distribution pattern can be

established for some experimental systems (e.g., in a fiber-matrix system). Both quantification methods are relatively easy to apply and they both show that the increase in EBSPs diffusiveness can be quantified for a low Z and polycrystalline aluminum.

#### **CONCLUSIONS**

The techniques for obtaining high quality electron back scattered patterns from bulk aluminum material using facilities available at the Department of Materials Science and Mechanics and MSU Computer Center have been developed. With thorough attention to the sample preparation, it should be possible to obtain EBSPs of equal or better quality from materials with larger atomic numbers and similar degrees of crystallinity. The results demonstrate conclusively that there is a continuous degradation of EBSP quality with increasing deformation. The pattern's diffuseness can be quantified using one and two dimensional Fourier transform methods. Of these, spectral first peak area (1-D) method appears to provide more consistent results, yet, without statistical proof, which requires large number of samples. These techniques allow plastic strain characterization at the micron-scale.

Two original experimental configurations have been optimized and evaluated; one for real-time measurements, the other for quantitative pattern evaluation. Both configurations utilize the image processing Semper 6.4 software, which was set up and fine-tuned during this research program. The practical approaches to optimize sample preparation, facilities, and processing of the images have been described in detail.

#### RECOMMENDATIONS

The most important hardware improvement would be the addition of a new high resolution, low light TV camera that would allow direct pattern capture. The analog-to-digital converter (ADC) attached camera should be able to guarantee 8-bit/ pixel transfer and resolution of 256 greyscale digitizing levels. The main criteria for the camera, ADC, and processing system is that the provided quality of in-PC imported pictures should be at least as good as those obtained with the currently used photo camera setup. This would result in both the necessary quality and real time pattern display.

For the present photo-camera setup, it may be advantageous to increase the EBSP capture angle by moving the film closer to the sample. Also, the setup should be rearranged so that patterns can be observed live using the TV system to adjudge the images prior to being captured using the 35mm film system.

For each material under consideration, it is critical to find the optimal sample preparation procedure to obtain high quality patterns. Machine shop access would be very important. The quantification using the Hough space may be helpful in some instances.

In the future it would be desirable to not only capture the images in real time, but also process the images in real time. This would allow the operator to instantly see the results and optimize the process of image acquisition. The easiest and most affordable way is a more powerful PC in addition to the improved camera. Alternatively, the existing PC could be set up as a server station to oversee the data distribution. In this setup, unloaded Case Center workstations or PCs could be used for processing the image frames. In this case, both the computer and the network should have transfer rates up to 30Mb/s.

# Appendix A

Correct semper.run file to account for European TV signal

```
page noprompt
type 'Welcome to Semper 6.4'
type
if batch jump warn
type 'The program in your run file (semper.run) is now being run;'
type 'as supplied, this attempts:'
type '
         (i) to assign a display device'
type '
         (ii) to assign a help library semper.hlb'
type '
        (iii) to assign a program file library, creating it if it does'
type '
            not already exist from semper.spl'
type '
        (iv) to assign a picture file pictures, creating it if it does'
            not already exist (500KB only, for test purposes)'
type '
type '
         (v) to read a test picture from semper.dat to CD:1, if no'
type '
            such picture already exists'
type '
         (vi) to display picture CD:1 in various ways'
type
type 'If anything goes wrong, type STOP and edit the run file as necessary'
type 'to do something more sensible before trying again; this program is'
type 'supplied for initial test purposes only, and users should eventually'
type 'establish their own startup programs to suit their own needs'
type
wait
type 'Enabling command echo to show you what is happening..'
type
echo commands terminal
assign display ccir
partitions:
! set initial current device; cd=n
! set depth of partitions; if nfr=3 fr2=3
partition 2 size 256 top left
partition 3 size 256 top right
partition 4 size 256 bottom left
partition 5 size 256 bottom right
partition 1
if nfr=3 unset fr2
lut 1 create; lut 2 create false; lut 3 create colour
erase frame; view frame
erase=yes
```

#### Appendix B

Semper image processing software summary

#### 1. SEMPER start-up and general management.

To start the Semper, switch on the PC and monitors, and click the Semper6.4 start-up icon in the Microsoft Windows 3.1' Applications folder or, if in DOS, type:

cd semper6p (makes the SEMPER6P directory current)

semper (starts the Semper software)

or, alternatively, semper /run=tutorial (to start the Semper tutorial software)

To end a session, type at the Semper prompt: end (same do the commands stop, quit, exit)

One can turn the power off either at the DOS prompt, or when in Windows.

First, Semper assigns devices and then gives the Semper prompt, S\$. Because pictures are stored on 'picture disks', it is convenient for each user to have their own picture disk, which can be assigned as the current device at the beginning of a session by command in

the following format at the Semper prompt:

assign name 'c:\Semper6p\UserDir\OperatorDisc'; cd=5

(Semper and MSDOS are not case sensitive, but the UNIX is).

Users who do not have their own picture disks can assign a temporary work disk:

assign scratch size 5000; cd=5

Semper provides a very useful help option. To get information about a command, type:

help <commandName>

e.g.: about histogram: help histogram

help histogram /full

(gives full available help about a command).

The content of the console display can be print on the adjacent dot matrix printer by applying the PrintScreen functional key on the PC keyboard.

The command partition defines the position and dimensions of the display partitions:

partition dis:3 size 256 top left

library partitions

One can find about the current Semper environment by typing: show devices

or, to examine the contents of the picture disc by typing: examine all

If Semper returns the message "Disc fragmented" when trying to create a new picture, one can compress a disc device, say the device 5, by grouping empty memory fragments together. The compressing can be done by typing at the prompt: compress device 5

#### 2. Image storage.

Semper refers to a picture by its number, say, 12, and by its device number. The latter by default is the number of the current device. The current device, say 5, is set by: cd=5 To see the picture 12 on the device 5, it is necessary to type the number:

5012 (just 12 if the cd=5).

The picture can be copied by *copy* or deleted by *del*, for more see *help < commandName >*.

#### 3. Image capture.

To capture frames into the whole screen area until a key or mouse button is pressed, one should use: live

With the wait command, it is possible to make SEMPER wait for fixed times, e.g.: wait 5 To copy display into picture #6 on disk with cd=5, type: copy display to 5006

To capture frames from the video input for 30 seconds using the real-time recursive filter. where a values from the range [0, 1] smooth the image and values from the range [-1, 0] live time a wait 30 sharpen it, type:

One can specify a destination partition and override the default scaling values by using the variables min and max and the option preset: min=0 max=200; live partition 2 preset

# 4. Image processing spatial-domain techniques

To plot a perspective display, where pixel intensity is plotted as surface height, one should Ymodulus 12

To create a picture intensity histogram, which shows the intensity ranges of picture pixels: histogram 12

To scale a picture so that the range, say, 15-50 becomes 5-250 (with maximum limits from 0-255, i.e., 256 gray scale levels), thus expanding the dynamic range of the picture (masking and stretching the histogram), one can write:

min=15 max=50; scale preset range 5, 250

It is convenient to perform arithmetical operations e.g.: difference of 2 and 3:

calculate:2-:3 to:4

One can get the brighter pixels of pictures 2 and 3 on display by typing: calculate max (:2,:3) to display

To level background variations one should subtract a fitted ramp of the form a\*x + b\*y. The ramps can be subtracted without its constant term (its value at the origin), preserving the background level at the origin:

fit 43 44 noconst subtract; expand 44; min=0, max=40; scale preset range 0,255

To extract regions (including arbitrary lines drawn with the mouse) of a picture: xwires section; extract from 1 to 2 @ section (line from the image 1 is extracted to #2) To extract a diagonal line through x,y for Fourier transformation, the following was used: extract 6 to 7 size 256,1 angle pi/4; pos x, y; display

To extract a square and mask it, so that a Fourier transformation can be performed: xwires; type x,y; extract size 256 @x,y; mask

It is possible to apply a high-pass filter to a picture, say #1. In order to do this, from each pixel the local mean over an arbitrarily large square block, say 40, is subtracted: hp 1 over 40 to 2

To search for points higher than the threshold one can use the command peaks. By default, peaks are stored in Plist 999. An example of application is as follows: extract 3 to 4 size 256,1; dis 4 to dis:1; peaks 4 to 5 threshold max\*0.4; mark dis:3 with t; type n

To print small blocks of pixels, say 7x5, around a position marked using the cursor: xwires; print @xy size 7,5

### 5. Local operations

To calculate for each pixel the local mean over a square block, say 20x20, one can use: *lmean display to 3 over 20* 

It is possible to smooth binary images, and, thus, to remove isolated pixels and lines. This option is just right for the needle-like noise of digital systems: *median display to 14*Rank applies a local ranking operator (3x3 or 5x5), achieving median filtering, erosion or dilation. The command ranks the pixels in the neighborhood of a given pixel in order of brightness and replaces it by the middle intensity value and removes the impulsive noise: *rank display*(3x3 median filter)

The command rf applies a two point separable recursive filter to a picture in all four directions in turn so as to smooth or sharpen with an infinite but symmetric point response. Values of the key a in the range [0, 1] smooth the image, and values in the range [-1, 0] sharpen it: rf 10 11 a .3

To change the value of any pixel in the currently selected picture, I used: pixel x, y, z=value, ivalue Similarly, to create a linear ramp in picture 1, I wrote:

create 1 size 256, 1; origin left; for x 0, 255; pixel x=x; loop

# 6. Semper frequency-domain commands (Fourier transformation).

The command fourier produces the discrete Fourier transform of a picture: fourier 3 to 4

The command image regenerates an image from a Fourier transform, i.e. performs the inverse transform:image 4 to 5

The command ps produces the power spectrum (the squared modulus of the Fourier transform, or diffraction pattern) of a picture; as an option, it can take the logarithm to compress the range:

ps 1 14 ln

The command fullplane calculates the full plane image, as the power spectrum of a real image is symmetrical and initially only the half plane is calculated.

One can use the command mask to reset all pixels inside/outside a given subregion to a constant or to perform low or high pass filtering of a Fourier transform. It is possible to give a 'soft-edge' to the mask.

The command survey reports the size, maximum, minimum, mean, and standard deviation of the pixels: survey 3 full

An example of calculations of Fourier transform of image 2: erase frame; display from 2 to dis:1 (displays 2)

mask from 2 to 4; display from 4 to dis:1

(mask off part of the image and displays)

fourier fro 4 to 5; ps from 5 to 6 ln; fullplane 6

(calculate the Fourier transform, power spectrum and the full plane image)

survey full 6; min=mean; display 6 to dis:2 preset

(gives thresholds, sets min, scales display)

An example of diffraction pattern display of picture 1 is shown below:

erase frame; display 1 to dis:1; mask 1 to 2 radiuss 110 width 10

(displays 1 and smooths edges)

ps 2 to 3; fullplane 3 (calculates power spectrum & full plane)

survey 3 (helps to determine threshold)

max=max/1000; dis 3 to dis:2 preset (sets saturation threshold and displays)
max=max/1000; dis 3 to dis:3 preset (compresses dynamic range more, displays)

The command window filters a Fourier transform so as to pass only pixels near the sites of a lattice defined by variables u and v, thereby eliminating most of the aperiodic noise.

This is an indirect way of effecting a lattice average: window 8 width .1

The command flc fits lattice Fourier components to local peak profiles in a Fourier transformation either individually or collecting the results for image regeneration. This, also, is an indirect way of effecting a lattice average:

u=15.6,23.4 v=-20.1,15.2 flc line 2,3 verify

(fits the peak with indices 2, 3)

flc 46 radius 200 to 47; image

(fits all peaks within 200 pixels of the origin).

# 7. Representative data exchange formats and hardcopy.

The command save dumps pictures to a newly created file with the same format as a normal Semper picture disc file. This is the most efficient way of saving pictures, e.g.: save 30 name 'emsa.sav'

The command write writes a picture to dynamically created file. While it is slow, it allows to write pictures in a form accessible to other programs or packages. One can use the command read to recover pictures that have been output with the write command:

write 4 name 'meltspin' < .dat=default extension>

read 5 name 'meltspin'

write 1 name 'binar.pic' unformatted <Fortran unformatt.>

read 2 unformatted name 'binar.pic'

write 2 format '(9F7.3)' name 'Al' <Al.dat in 9F7.3>

One can use the command output to output pictures and the command input to read pictures from files in the raw/fast binary (\*.bin, \*.pbm, \*.pic), in the PC Paintbrush greyscale PCX (\*.pcx), or in the Media Cybernetics CUT (\*.cut) file formats:

output 7 raw name 'a:\bs.bin' <raw binary, byte stream>

input 8 raw name 'a:\bs.pbm' size 99,95

output 23 name 'binary' <fast binary; \*.pic=default extension>

input 24 name 'binary'

output 102 paint name 'PAINT.pcx <Paintbrush, \*.pcx=default extension>

input 103 paint name 'PAINT.pcx'

output 11 new cut name 'DrHalo.cut' <CUT, \*.cut=default extension>

input 12 cut name 'DrHalo.cut'

It was found that the raw binary format is the most appropriate data exchange format for this project. However, when using this format it is critical to know the image size in pixels. The command title replaces the title recorded with a picture:

title text 'Frame ',n,' with background levelled'

The command postscript writes out Semper images or screen dumps in the \*.ps format. Postscript files can be sent to a PostScript printer, which can handle large size print jobs, e.g., eb119\_ps2: postscript 5 name 'a:\FeAl.ps' times 2 text 'EBSP from FeAl' (creates a \*.ps file of the picture #5, magnified by 2)

overlay white; ymodulus 17 to display; post part dis name 'a:\Ym.ps' (creates a \*.ps file of Ymodulus).

To copy the FeAl.ps file from a MSDOS disk into UNIX, type a the UNIX prompt: mcopy a:FeAl.ps FeAl.ps

To see the file in the UNIX use the *Is* or *II* commands. To see the FeAl.ps file, the ghostscript software should be used: *gs FeAl.ps* 

To change the layout dimensions, the header of a \*.ps file might be edited with a text editor. To print the file, type: <code>lpr-Peb119\_ps2 FeAl.ps</code> at the UNIX prompt. To see the status of the eb119\_ps2 printer-job queue, I type: <code>lpstat-oeb119\_ps2</code> On UNIX machines, one can access the image editor xv, by typing: xv at the UNIX prompt. This editor was mostly used to transform files in different file formats. On the Case Center's SUN workstations it is possible to copy the UNIX file, such as bs.pbm (raw), onto a MSDOS 3" disk by: mwrite bs.pbm a:bs.pbm and to see the contents of the disk in the SUN UNIX workstation drive by: mdir a: The IP address of the Semper PC is 35.9.35.125, and name semper.egr.msu.edu

# Additional Semper usage notes.

It is possible to recall a used Semper command back at the system prompt for new usage by using the black arrows on the right side of the PC keyboard. The command ratio can correct the image elongation on the image display, due to two video standards (American NTSC and European CCIR (PAL)) used by the hardware in the experimental setup: expand 12 to display ratio 4,5 Yet, the system is set so, that images can be stored, printed, and exchanged without problems, thus, normally, the command ratio is not used to get a circular image on the image display.

# Appendix C

Live EBSP capture and processing Semper commands used

- ! Live-capture the images into Semper. live time 1 wait 30; copy dis to 1
- ! Remove the background ramp and stretch the image over the 256 greyscale levels fit 1 2 subtract noconst; 2; min=mean-3\*Sd max=mean+3\*Sd; scale preset range 0, 255; 2
- ! The following steps sometimes may be found useful
- ! Simulate picture background by obtaining 40 x 40 pixel mean for each pixel lmean 2 to 3 over 40; 3; scale preset range 0, 255; 3
- ! Copy binary pictures 2 and 3 into integer pictures 4 and 5. copy 2 4 int; copy 3 5 int
- ! Subtract the background. Display the resulting pattern.

calculate :4 - :5 to 6; 6; survey full 6

! Try median filtering to the resulting picture. median 6 7; 7; survey full 7

#### Appendix D

## 1-D SFPA quantification Semper comands used

```
Get the images into Semper. Write protect image.
input 1 raw name 'a:\eb00Al.bin' size 288,432; 1; wp 1
       Find the point around which to extract and extract a 256x256 pixel square
1; xwires; type x,y; extract size 256 @x,y to 2; 2; survey full 2
       Remove the background ramp and stretch the image over the 256 greyscale levels
fit 2 3 subtract noconst; min=mean-3*Sd max=mean+3*Sd; scale preset range 0, 255; 3
       Copy binary picture 3 into an integer picture 4. Reset the mean to zero
copy 3 4 int; survey full 4; calculate :4 - mean to 5; 5
       Extract and average the displayed picture along a direction indicated with cursor
       Sometimes smaller than 256,1 size may be necessary
xwires line; project 5 6 angle theta average; extract 6 7 size 256,1
       Subtract the image mean value from the image
survey full 7; 7; wp 7; calculate :7 - mean to 8
       Create the Hanning function 98 and with it weight the image 7
create 98 size 256, 1; calculate 0.5*(1+cos(2*Pi*x/256); weight 8 with 98 to 9; 9
       Next, calculate the FT and the halfplane PS
ps 10 12; wp 12; 12
       See what the picture is like and find at which pixel the first maximum ends
12; survey full 12; max=max/40; dis 12 size 20 left times 30; print 12 left; print 12 right
       Find area, A1, under the first peak of PS
A1=0; for x 0,3; A1=A1+p(x); loop; type A1
       Find total area, B1, under the PS
B1=0; for x 0, 128; B1=B1+p(x); loop; type B1
       Find SFPA = A1/B1
SFPA=A1/B1; type SFPA
```

## **Appendix E**

# 2-D PSFM quantification Semper comands used

```
Get the images into Semper. Write protect the image
input 1 raw name 'a:\eb00Al.bin' size 288, 432; 1; wp 1
       Find the point around which to extract and extract a 256x256 pixel square
1; xwires; type x,y; extract size 256 @x,y to 2; 2; survey full 2
       Remove the background ramp and stretch the image over the 256 greyscale levels
fit 2 3 subtract noconst; min=mean-3*Sd max=mean+3*Sd; scale preset range 0, 255; 3
       Copy binary picture 3 into an integer picture 4. Reset the mean to zero
copy 3 4 int; survey full 4; calculate :4-mean to 5; 5
       Create the Hanning function and weight image 5 with it
create 98 size 256, 1; 98; calculate 0.5*(1+cos(2*Pi*x/256); weight 5 with 98 to 8; 8
       Remove the background ramp.
fit 8 9 subtract noconst
       Bring the mean intensity to zero
survey full 9; calculate :9-mean to 10 int; 10; survey full 10; wp 10
       Next, calculate the FT and the fullplane PS
ps 10 12; fullplane 12; wp 12
       See what the picture looks like and find at which pixel the first maximum ends
12; survey full 12; max=max/40; display 12 size 40 times 10
       Find 1-D PS, formed by integrating 2-D PS
12; section to 14; display 14 size 20 left times 30; survey full 14; wp 14; print 14 left
       Find area, B2, under 1-D PS, formed by integrating 2-D PS at each frequency
B2=0; for x 0,181; B2=B2+p(x); loop; type B2
       Create 1-D linear ramp function in picture 97
create 97 size 182,1; calculate x+ 91; 97
       Weight the frequency averaged 1-D PS with radiuss
weight 14 with 97 to 15; survey full 15; 15; wp 15
       Find area, A2, under radiuss weighted, f-cy averaged 1-D PS
A2=0; for x 0, 181; A2=A2+p(x); loop; type A2
       Find PSFM = A2/B2
PSFM=A2/B2; type PSFM
```

# **LIST OF REFERENCES**

#### LIST OF REFERENCES

- 1. J.A. Venables and C.J. Harland, *Phil. Mag.*, **27** (1973) 1193
- 2. C.J. Harland, P. Akhter, and J.A. Venables, J. Phys., E14 (1981) 175
- 3. V. Randle, B. Ralph, and D.J. Dingley, Acta. Metall. Mater., 36 (1988) 267
- 4. D.J. Dingley and K. Baba Kishi, Scanning Electron Microscopy, II (1986) 383
- 5. J. Hjelen, R. Orsund, and E. Nes, Acta. Metall. Mater., 39 (1991) 1377
- 6. D.J. Dingley and V. Randle, J. Mater. Sci., 27 (1992) 4545
- 7. A.J. Wilkinson, Mater. Sci. Eng., A135 (1991) 189
- 8. A.J. Wilkinson and D.J. Dingley, Acta. Metall. Mater., 40 (1992) 3357
- 9. K.Z. Troost, P. van der Sluis, and D.J. Gravenstein, Appl. Phys. Lett., 62 (1993) 1110
- 10. B.D. Cullity. Elements of X-ray Diffraction, 2nd, Addison Wesley Publ. Co, 1978
- 11. **SEM microcharacterization of semiconductors**, Techniques of Physics : 12.,
- ed. D.B. Holt and D.C. Joy, Academic Press, 1989
- 12. P.B. Hirsch and C.J. Humphreys. (1970). In *Scanning Electron Microscopy/1970*, Chicago, 449
- 13. C.J. Rossouw, P.R. Miller, T.W. Josefsson, and L.J. Allen, *Phil. Mag. A*, **70** (1994) 985
- 14. A.B. Laponsky and N.R. Whetten, Phys. Rev. Lett., 3 (1959) 510
- 15. O.C. Wells. (1976). In Use of Monte Carlo Calcul. in Electron ProbeMicroanalysis and Scanning Electron Microscopy, ed. K.F. Heinrich, NBS Special Publication 460, 139
- 16. D.E. Newbury, D.C. Joy, P. Echlin, C.E. Fiori, and J.I. Goldstein, *ibid*, 151
- 17. D.E. Newbury, H. Yakowitz, and R.L. Myklebust, Appl. Phys. Lett., 23 (1973) 448

- 18. D.E. Newbury and R.L. Myklebust. (1984). In *Electron Beam Interactions with Solids*, SEM, Inc, Chicago, 153
- 19. K.F. Heinrich. Electron Beam Microanalysis, Van Nostrand, New York, 1981, 245
- 20. G.G. Hembree, S.W. Jensen, and J.F. Marchiando. Microbeam Analysis, San Francisco Press, 1981, 123
- 21. P.B. Hirsch, A. Howie, R.B. Nicholson, D.W. Pashley, and M.J. Whelan. **Electron Microscopy of Thin Crystals**, 2nd, Krieger, New York, 1978
- 22. P.J. Goodhew. Specimen Preparation for Transmission Electron Microscopy of Materials, Oxford University Press, London, 1984
- 23. **Practical Methods in Electron Microscopy**, Vol. 1., ed. A.M. Glauert, N.Y. American Elsevier Publishing Co, Inc., 1972
- 24. J.I. Goldstein, D.E. Newbury, P. Echlin, D.C. Joy, C.E. Fiori, and E. Lifshin. Scanning Electron Microscopy and X-ray Microanalysis, Plenum Press, New York, 1992
- 25. Gerjan Van Bakel's e-mail message. (1994). (article #331 of the sci.techniques.microscopy Usenet newsgroup)
- 26. A. Rose. (1948). In Advances in Electronics, ed. A. Marton, Acad. Press, N.Y., 131
- 27. A. Rose, Image Technology, June/July (1970) 13
- 27. R.C. Gonzalez and P. Wintz. **Digital Image Processing**, 2nd ed., Addison-Wesley, 1987
- 29. John Francis Mansfield's e-mail message. (1994). (article #333 of the sci.techniques.microscopy Usenet newsgroup)
- 30. K.Z. Troost, P. van der Sluis, and D.J. Gravensteijn, Appl. Phys. Lett., 62 (1993) 1110
- 31. J.L. Harris. (1968). In Eval. Motion Degraded Images, NASA Publ. SP-193, 131
- 32. B.R. Hunt. (1973). The Application of Constrained Least Squares Estimation to Image Restoration by Digital Computer. *IEEE Trans. Comput.*, C-22 9 (1973) 805
- 33. E.R. Meyer and R.C. Gonzalez, R.C. (1983). In *Proc. First South Afr. Symp. Digital Image Proc.*, Univ. of Natal, Durban, South Africa, 137
- 34. A.J. Wilkinson and D.J. Dingley, Acta. metall. mater., **39** (1991) 3047

- 35. O. Brigham. The Fast Fourier Transform, Prentice-Hall, 1974
- 36. R. Bracewell. The Fourier Transform and its Applications, Mc Graw-Hill, 1965
- 37. A. Papoulis. The Fourier Integral and its Applications, Mc Graw-Hill, 1962
- 38. J.W. Dally. W.F. Riley, K.G. McConnell. (1993). Instrumentation for engineering measurements, 2nd ed., John Wiley & Sons, Inc
- 39. A.J. Wilkinson. (1995) (personal communication)
- 40. A.W. Gibson. (1995). Master's Thesis, Michigan State University
- 41. Accustom-5 Instruction Manual No: 14947001 in A234EB. (1994). Struers, Copenhagen, Denmark
- 42. L.E. Samuels. Metallographic Polishing by Mechanical Methods, Pitman, Belfast, Ireland, 1971
- 43. J.L. Whitton, *Proc. Roy. Soc.*, A. **311** (1969) 63
- 44. SEMPER manuals
- 45. AN10000 EBSP manual AN10-EBS-0288, Link Analytical, Bucks, England
- 46. F.W. Young, Jr. and T.R. Wilson, Rev. Sci. Instr., 32 5 (1961) 559
- 47. M.D. Hunt, J.A. Spittle, and R.W. Smith, J. Sci. Instr., 44 (1967) 230
- 48. T. Broom and J.M. Summerton, J. Sci. Instr., **36** (1959) 245
- 49. U. Bonse, E. te Kaat, and E. Kappler, J. Sci. Instr., 42, (1965) 631
- 50. I.A. Bucklow and M. Cole, Met. Rev., 14 (1969) 103
- 51. A. Gibson, O. Balcers, and M.A. Crimp, submitted to J. Microscopy, (1995)
- 50. J. Russ and D. Bright, J. Comp. Assist. Microsc., 1 (1) (1989) 1
- 51. D.J. Dingley and Karim Baba-Kishi, Microscopy and Analysis, May (1990)

